

Article

# He-Ar Isotopes and Trace Gas Compositions of Fluid Inclusions in Massive Sulphides from the Yushui Copper-Polymetallic Deposit, South China: Metallogenic Implications

Yi Huang <sup>1,†</sup>, Zhongwei Wu <sup>2,3,†</sup>, Xiaoming Sun <sup>2,3,4,5,\*</sup> , Yan Wang <sup>1</sup>, Guiyong Shi <sup>2,3,5</sup>, Wei Zhai <sup>2,3,5</sup> and Yao Guan <sup>6</sup> 

<sup>1</sup> South China Sea Institute of Planning and Environmental Research, State Oceanic Administration, Guangzhou 510300, China; hygyouxiang@126.com (Y.H.); we85289786@163.com (Y.W.)

<sup>2</sup> School of Marine Sciences, Sun Yat-sen University, Guangzhou 510006, China; figowzwpig@163.com (Z.W.); eessgy@mail.sysu.edu.cn (G.S.); eeszw@mail.sysu.edu.cn (W.Z.)

<sup>3</sup> Guangdong Provincial Key Laboratory of Marine Resources and Coastal Engineering, Guangzhou 510006, China

<sup>4</sup> School of Earth Sciences and Engineering, Sun Yat-sen University, Guangzhou 510275, China

<sup>5</sup> Southern Marine Science and Engineering Guangdong Laboratory (Zhuhai), Zhuhai 519000, China

<sup>6</sup> Fourth Institute of Oceanography, Ministry of Natural Resources, Beihai 536000, China; guanyao@mail2.sysu.edu.cn

\* Correspondence: eessxm@mail.sysu.edu.cn; Tel.: +86-020-84110968

† These authors contributed equally to this work.

Received: 29 March 2019; Accepted: 24 April 2019; Published: 29 April 2019



**Abstract:** The Yushui ore deposit, located in the middle section of the Yong'an-Meixian Hercynian depression, is a medium-sized Cu-polymetallic massive sulphide deposit in Eastern Guangdong Province, South China. This deposit is characterized by unusually high copper grade (up to 50–60 wt. % Cu). Other metallic elements, such as lead, zinc and silver, are also economically important in the Yushui ore bodies. The aim of this study was to apply N<sub>2</sub>–Ar–He systematics, together with organic gases (light-hydrocarbon tracers), to constrain the origin and evolution of ore-forming fluids. The helium-argon isotopes and trace gas compositions of fluid inclusions trapped within metal sulphide minerals were measured for a number of bonanza ores from the Yushui deposit. The noble gas concentrations in the studied samples vary over one to two orders of magnitude (<sup>4</sup>He: 2.27–160.00 × 10<sup>−5</sup> cm<sup>3</sup> STP g<sup>−1</sup>; <sup>3</sup>He: 0.53–34.88 × 10<sup>−12</sup> cm<sup>3</sup> STP g<sup>−1</sup>; <sup>40</sup>Ar: 6.28–37.82 × 10<sup>−7</sup> cm<sup>3</sup> STP g<sup>−1</sup>; <sup>36</sup>Ar: 1.25–10.40 × 10<sup>−9</sup> cm<sup>3</sup> STP g<sup>−1</sup>). Our data show a narrow range of <sup>3</sup>He/<sup>4</sup>He ratios from 0.006 to 0.056 R<sub>a</sub> (~0.026 R<sub>a</sub> on average, n = 8), which are considerably lower than the modern atmospheric end-member value; whereas the <sup>40</sup>Ar/<sup>36</sup>Ar ratios (ranging from 333.76 to 501.68, with an average of 397.53) are significantly greater than that of air-saturated water. Most of the bornite samples have somewhat higher <sup>3</sup>He/<sup>4</sup>He ratios of trapped fluids when compared to chalcopyrite. Overall, these He-Ar results are well within the range of crustal reservoir, thus implying a predominantly crustal source (originated from Caledonian basement) for ore-forming solutions, with little contribution from mantle-derived fluids. Analysis of the N<sub>2</sub>–Ar–He composition in Cu-rich sulphides indicates that the Yushui ore-forming fluids were probably derived from formation water (or basinal hot brines). Moreover, organic gas species identified in sulphide-hosted fluid inclusions are mainly composed of C<sub>1</sub>–C<sub>4</sub> alkanes, while the concentrations of unsaturated olefins and aromatic hydrocarbons are very low. In particular, most chalcopyrite samples with relatively low <sup>3</sup>He/<sup>4</sup>He ratios (0.006–0.016 R<sub>a</sub>) and <sup>40</sup>Ar/<sup>4</sup>He values (0.0002–0.0012) are generally characterized by very high CO<sub>2</sub>/CH<sub>4</sub> ratios (~60–102). All these suggest that main-stage Cu-Ag metallogenic processes might have not been affected by high-temperature magmatic activities or superimposed by strong metamorphic overprinting, although some chalcopyrite-rich ores appear to be influenced by later

stage hydrothermal processes. In summary, neither magmatic input nor convecting seawater has played an important role in the formation of Yushui copper-polymetallic deposit. The massive sulphide ore bodies were products of water–rock interaction between metal-bearing basinal brines and the host sedimentary strata.

**Keywords:** He–Ar isotopes; N<sub>2</sub>–Ar–He compositions; light hydrocarbon gases; ore-forming fluids; Yushui copper-polymetallic deposit

---

## 1. Introduction

The most important base-metal ore fields in South China are represented by a number of sediment-hosted, stratabound massive sulphide deposits, which mostly occur within a series of Late Palaeozoic (Hercynian–Indosinian) intracontinental rift basins [1]. Among these deposits, the Yushui ore deposit is one of the most Cu-rich massive sulphide deposits yet found in Southern China [1–3]. It is located in the eastern Nanling metallogenic belt, about 13 km away from Meixian County of Guangdong Province. Being a medium-sized Cu-polymetallic deposit, this deposit is also high in Pb, Zn and Ag, as well as rare earth elements (REEs) [2–5]. First discovered in the late 1980s, the Yushui deposit has attracted considerable attention and research interest from Chinese economic geologists, owing to extremely high copper grades of its ore bodies (approximately 3.25% Cu on average) formed in a small area (~0.2 km<sup>2</sup>) [2–12]. In some of the richest bonanza ore bodies, their typical grades can even reach as high as 50–60 wt. % Cu, with recoverable Ag (up to 10,000 ppm) [11,13]. By contrast, average ore grades of most copper deposits in China are generally low (~0.87 wt. % Cu) [14]. In other words, the Yushui ore deposit represents one of only a few unique examples of polymetallic massive sulphide deposits that contain some of the highest levels of Cu and Ag ever reported in southern China [1]. Therefore, comprehensive studies of this deposit can guide further exploration for a similar style of Cu–Pb–Zn–(Ag) mineralization in the Nanling Region.

However, the genesis and ore-forming mechanism of the Yushui Cu-polymetallic deposit has been somewhat controversial over the past thirty years [1–3,5,8–12]. Although once regarded as a sedimentary exhalative (SEDEX) or Mississippi Valley-type (MVT-like) deposit [2,10,12], it was thought to be of magmatic-hydrothermal origin at first, because of the observed phenomenon that its host strata were commonly intruded by Mesozoic diabase dykes and granitoids [3,8]. Some authors have also proposed that this deposit was originally formed by ancient (Late Palaeozoic) submarine exhalation-sedimentation and was then transformed/superimposed by Yanshanian diabase or granitoid intrusions as well as related hydrothermal fluids [5]. Although this view has been widely accepted by many researchers [1,11,15], the major source of ore-forming fluids still remains to be a matter of continuing debate [8,12]. This research focuses on whether the metal-bearing solutions were mainly derived from the Yanshanian magmatic-hydrothermal fluids or originated from the mixture of deep-/shallow-circulating meteoric water (or seawater) and old Caledonian basement components during a Carboniferous syn-sedimentary exhalative hydrothermal event. Furthermore, the composition of trace gases in fluid inclusions trapped in the Yushui sulphide minerals and the evolution of ore-forming fluids through multiple stages of polymetallic mineralisation are also poorly understood.

To address the above-mentioned questions, the application of noble gas (especially helium and argon) isotope geochemistry is key to defining the origin of ore-forming fluids. In particular, as a monatomic chemically inert gas (<sup>3</sup>He behaves extremely conservatively during mixing of mantle-/crustal-derived fluids with meteoric water), helium is considered to be one of the most sensitive geochemical tracers for such studies and has distinct isotopic signatures in different types of geological reservoirs [16–34]. For ancient polymetallic ore deposits, the He–Ar isotopic compositions of hydrothermal fluids are faithfully preserved when trapped as fluid inclusions by mineral phases such as pyrite, chalcopyrite, sphalerite, or galena, and thus can be widely used to reveal the degree of

fluid-rock interaction, mantle degassing or magmatic activity [35–47]. Additionally, quantitative bulk sample analysis of the ratios among conservative trace gas species  $N_2$ , Ar, and He can help to estimate the amounts of magmatic, crustal and meteoric gaseous constituents in geothermal fluids [48–55]. Moreover, the concentrations and distribution features of light organic compounds (LOC, including methane) in fluid inclusions from a variety of hydrothermal systems or massive sulphide deposits can also serve as an important and powerful tool to interpret the various sources of organic species, as well as to illustrate fluid boiling/mixing processes, and provide useful information about the intensity of wall-rock alterations [56–66]. Therefore, an integrated study of the He-Ar isotopic systematics, combined with the  $N_2$ -Ar-He or  $CH_4/CO_2$  ratios of fluid inclusion volatiles, allows us to further develop our understanding of fluid evolution and metallogenic processes in the Yushui copper-polymetallic ore deposit, South China.

## 2. Geological Setting

### 2.1. Regional Background of the Yushui Deposit

The Yushui copper-polymetallic deposit is located in the middle section of the Yong'an–Meixian Late Paleozoic Hercynian depression. The Zhenghe-Dapu and Shaowu-Heyuan regional faults (formed in an extensional tectonic setting induced by lithospheric thinning and asthenospheric upwelling) [67] comprise the east and west boundaries of the depression zone, respectively. As shown in Figure 1A, this NNE-trending depression is approximately 500 km long and 150 km wide. It extends from Jiangle and Yong'an (Fujian Province) at its north end to Huizhou (Guangdong Province) in the south. The regional geological evolution is considered to have occurred in three stages: (1) passive continental margin, (2) part of the Cathaysia Block (or defined as South China Caledonian-aged fold belt), and (3) active continental margin [68–70]. During the Sinian-Early Paleozoic period (ca. 750–500 Ma), this region was part of the Proto-Tethys Ocean. Before the Middle Cambrian, a geosynclinal depression filled with thick (>2000 m) flyschoid units had been formed in the study area. The southern part of the Proto-Tethys Ocean was gradually closed in the early Paleozoic, which might be linked to the Wuyi-Yunkai orogeny in South China (460–415 Ma) [71]. As a result, the sedimentary sequence was folded and then uplifted, leading to the formation of a basement with the absence of younger rocks (the Ordovician to Lower Devonian) in this region. During the Devonian–Middle Triassic, a paraplatform environment developed with an entire cycle of transgression and regression. The transgression peaked in the Late Carboniferous, and then a shallow-marine carbonate platform formed. Afterwards, regional extension resulted in a series of steep faults along the pre-existing basement structure with a NE-ESE trend. In the Middle–Late Triassic, this region became an active continental margin during the period of Indosinian tectonic movement (ca. 250–200 Ma) [11,72].

The regional stratigraphy is subdivided from bottom to top into five units (Figure 1B).

- (1) Middle Devonian–Lower Carboniferous ( $D_2$ - $C_1$ ): primarily medium- to fine-grained quartz sandstone, pebbly quartz sandstone, conglomerate with thin-bedded mudstone and siltstone, representing clastic rock formation characterized by neritic-littoral facies. This set of strata tilt to the northeast, with a dip angle of 25 to 30 degrees and a thickness greater than 300 m [73].
- (2) Upper Carboniferous Hutian Group ( $C_{2ht}$ ): dominated by dolomite with dolomitic limestone and limestone, or accompanied by thin layers of irregular light-colored chert, quartz sandstone, and mudstone, suggesting a neritic to littoral facies of carbonate rocks, overlying the Middle Devonian–Lower Carboniferous clastic rocks with a low-angle unconformity and a thickness of 200 to 350 m [73].
- (3) Upper Jurassic Gaojiping Group ( $J_{3gp}$ ): continental volcanic rocks, mainly consisted of mafic, intermediate to felsic lavas and clastic rocks overlying the Upper Carboniferous Hutian Group (with a nearly parallel, eruptive unconformity); approximately 30–80 m in thickness.

- (4) Lower Cretaceous Guancaoahu Group ( $K_1gn$ ): represented by lacustrine volcano-sedimentary clastic rocks (with purple-red color), overlying the Upper Jurassic Gaojiping Group with an angular unconformity. The strata tilt to the north with a thickness of 150–200 m.
- (5) Quaternary (Q): eluvium, alluvium, and diluvium.

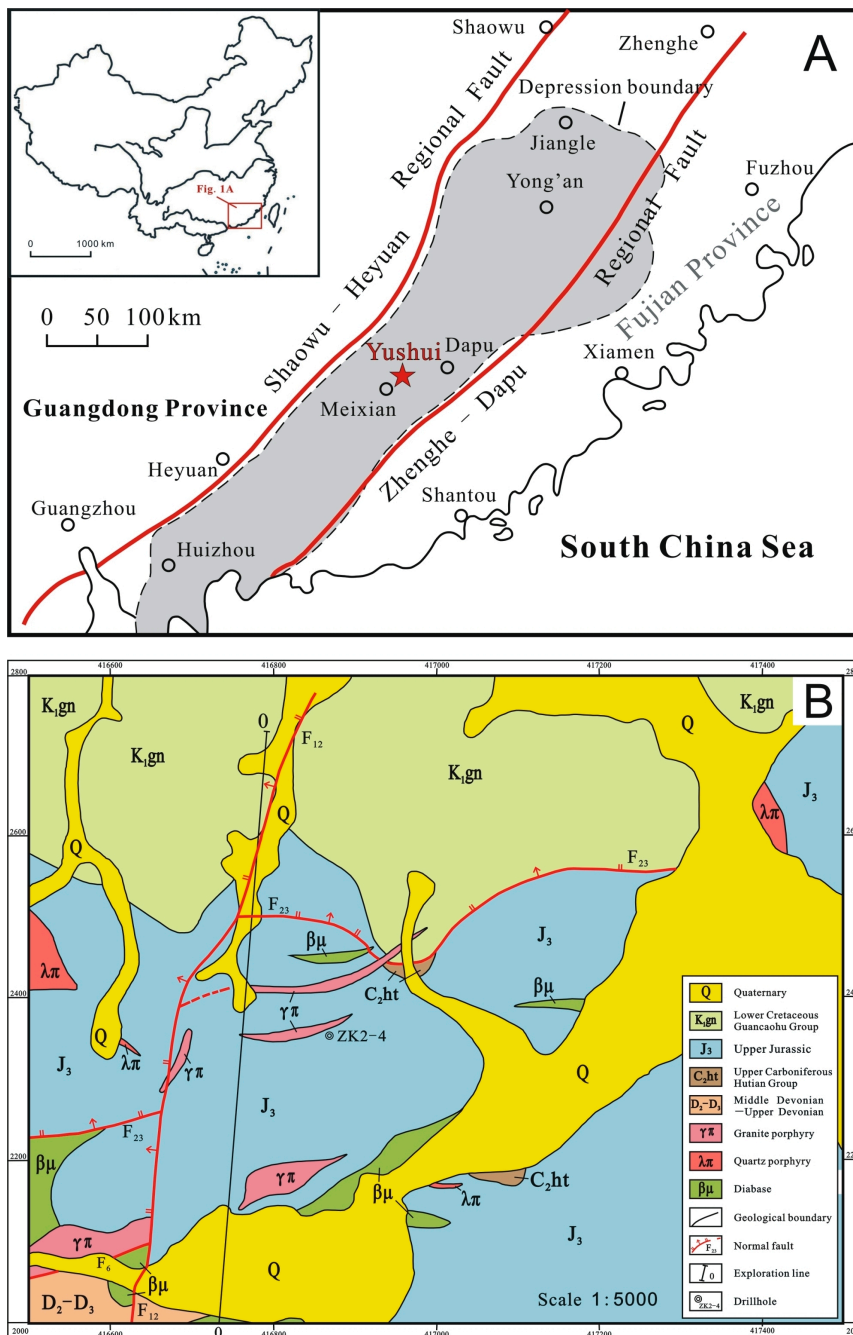


**Figure 1.** Schematic geological maps of the Yushui copper-polymetallic massive sulphide deposit in Meixian County, Guangdong Province. (A) Location map of the Yushui ore deposit in the middle section of the Yong’an–Meixian depression zone (modified after [2]). Inset shows regional setting of the study area in the Nanling Region, South China; (B) Regional stratigraphy of the Yushui mining district (modified after [2], data sources from No. 723 Geological Prospecting Team and the local mining company). Note that the deeply concealed ore bodies are hosted in the sedimentary strata of Upper Carboniferous Hutian Group and Lower Carboniferous Zhongxin Formation (not marked on this map).

Although there is no distinct folding observed in the mining district, fault structures were well developed owing to the influence of regional tectonics. These deep faults are E–W, NE–SW, and NW–SE trending. Fault  $F_{23}$  (with a dip angle of  $75^\circ$  to  $85^\circ$ ) was the main ore-controlling structure for the Yushui copper-polymetallic deposit. This large normal fault formed during the Devonian–Carboniferous period, with NW side downthrown and SE side upthrown. The subvertical  $F_{23}$  fault plane was distorted along its strike or dip direction, which is spatially close to the main ore bodies. Additionally, igneous rocks present in this district (including diabase, granite porphyry and minor quartz porphyry) mostly intruded along the three fault sets. The diabasites, with a K–Ar age of  $\sim 150$  Ma [2,3], occur as irregular dykes and commonly cut through the ore bodies (Figure 2a). They are often found in underground workings, but rarely in outcrops. The diabase dykes have an ophitic texture, and are mainly composed of pyroxene and plagioclase. These dykes are prone to alteration, such as carbonatization, chloritization, silicification, and sericitization. Weakly altered reddish, porphyritic granite occurs in the mining area or underground workings. Phenocrysts within the granite porphyry are dominantly potassium feldspar, quartz, and minor biotite and plagioclase. The groundmass is made up of felsic minerals, such as plagioclase, potassium feldspar, and quartz.

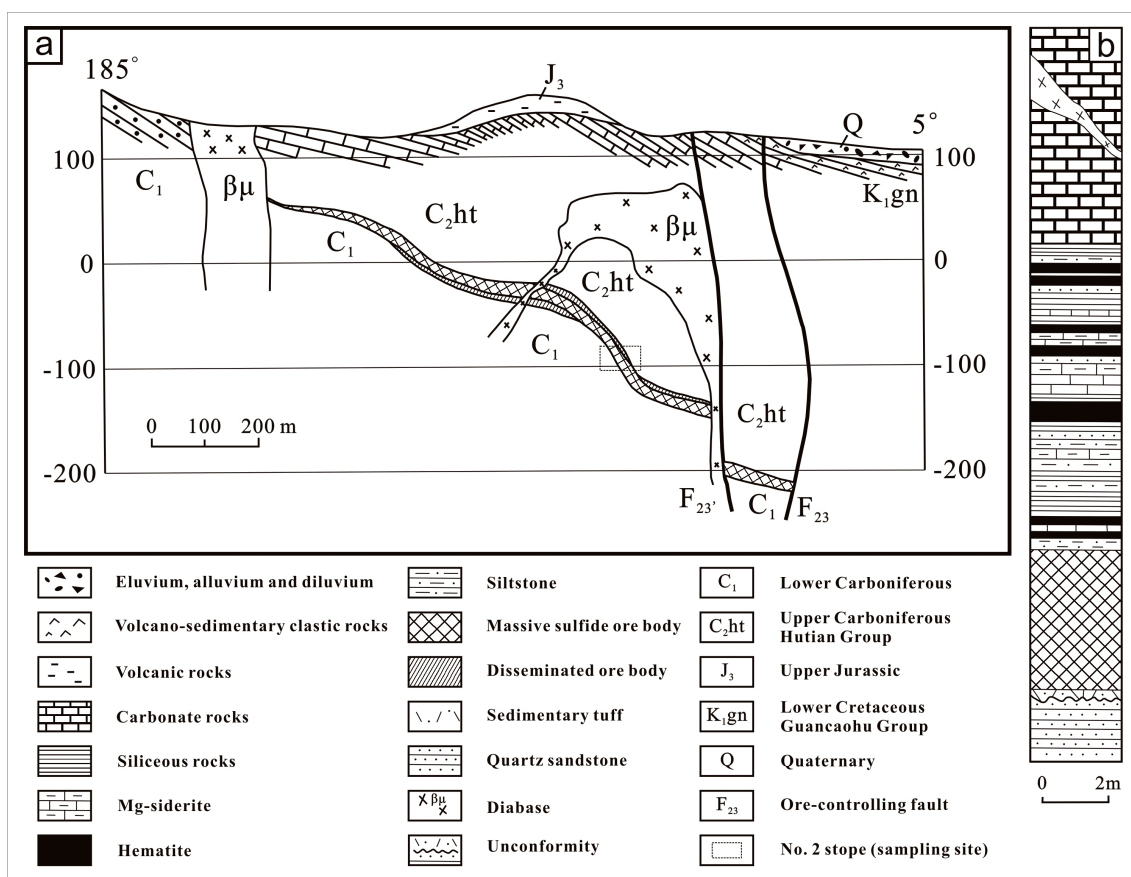


**Figure 2.** Geological profiles of the Yushui copper-polymetallic deposit (a) Cross section of ore-bearing sector along No. 0 exploratory line; (b) columnar section of No. ZK2-4 drillhole (modified after [1,10]). Note that the locations of No. 0 exploratory line and No. ZK2-4 drillhole are both marked in the map of regional stratigraphy shown above (Figure 1B).

### 2.2. Occurrences and Distribution of Ore Bodies

The ore bodies of the Yushui Cu-polymetallic deposit appear in bedded/stratiform, lenticular and vein-like shapes, containing about 99,000 tons of copper, 182,600 tons of lead, and 333 tons of silver [11]. With a thickness of 0.1–19 m, the ore horizon is situated at the unconformity interface between the

limestone of the Upper Carboniferous Hutian Group and the quartz sandstone of the Lower Carboniferous Zhongxin Formation (Figure 2a). The Yushui ores are mainly characterized by massive, disseminated, stockwork and lamellar structures, exhibiting paragenetic, exsolution, metasomatic and/or crushed texture. The ore-mineral assemblages are dominantly composed of bornite, chalcopyrite, chalcocite, galena, sphalerite, and pyrite, with trace amounts of argentite/acanthite, siegenite, and Ag-bearing sulphosalts. Gangue minerals are dominated by quartz, calcite, sericite and chlorite. The main ore bodies consist of three layers, which are described from bottom to top as follows (Figure 2b):

- (1) Ore-bearing tuffaceous sedimentary layer, with a thickness of 5–30 cm. The tuffaceous sedimentary rocks occur interbedded with thin layers of Cu-rich sulphide ores, showing microlaminations. Feldspar and quartz occur as phenoclasts in the tuffaceous layers. This layer unconformably overlies the Carboniferous clastic rocks.
- (2) Bedded/stratiform massive sulphides, with a thickness of 0.1–9.4 m. This layer has the highest Cu grade locally reaching more than 50 wt. %. Silver occurs predominantly in the copper-rich ores and exhibits a positive correlation with Cu grades (but not with Pb or Zn contents) [13]. The grain sizes of sulphide minerals are very fine (mostly less than 0.1 mm), displaying laminated structures. Moreover, flow structures and plastic deformation can also be observed in such laminated layers [2,3,73].
- (3) Hematite–chert layer, closely associated with the massive sulphide ores, 0.1–3.7 m in thickness. It is a mixed sedimentary layer with very fine intercalations of exhalative materials and sediments. The hematite-bearing chert/siliceous mudstone locally occurs with siderite, siltstone, (sandy) dolomite, and more rarely thin-bedded sulphide ore layer. All these geological characteristics mentioned above indicate that the Yushui copper-polymetallic deposit has the typical features of a seafloor sedimentary-exhalative deposit [1,15,74,75].

Overall, hydrothermal alteration within the hanging-wall strata is rather weak, with slight silicification as well as Pb-Zn mineralization and pyritization. Comparatively, the footwall alteration is more pervasive, with carbonatization, chloritization, sericitization and Cu-Pb-Zn-(Ag) mineralization. Furthermore, the intensity/degree of alteration gradually decreases from top downwards.

### 3. Sampling and Analytical Methods

A number of massive sulphide samples were collected from the –100 m level of No. 2 stope in the Yushui deposit (Figure 2a). These typical massive sulphides were formed during the main mineralization stage, and are principally composed of massive bornite ores (including the richest Cu-Ag bonanza), massive chalcopyrite or galena-dominated ores, as well as mixed ores of bornite and chalcopyrite (as shown in Figure 3a–f). Some of the samples contain interpenetrating veins of galena, sphalerite, and calcite. Reflected-light photomicrographs of polished thin sections show that in the Pb-Zn-rich ore samples, colloform or irregular-shaped sphalerite aggregates occur as coarse-grained inclusions enclosed within massive porous galena (Figure 4a); whereas in Cu-rich bonanza ores, anhedral bornite and/or chalcopyrite aggregates commonly occur as intimate intergrowths with sphalerite, pyrite or chalcocite (Figure 4b–e), but most of these Cu-Fe sulphide crystals rarely coexist with disseminated phyllosilicates or other clay minerals. In some cases, minor amounts of sphalerite and bornite are present as fine-grained inclusions disseminated throughout the chalcopyrite matrix (Figure 4f).

By using agate mortar and pestle, selected ore fragments of representative hand specimens ( $n = 8$ ) were roughly crushed into millimeter-sized granules. To obtain homogeneous microcrystalline groundmass separates, various types of metal sulphides with small diameters (20–60 mesh size fractions), such as bornite, chalcopyrite and galena, were sieved and carefully hand-picked under a binocular microscope at Guangdong Provincial Key Laboratory of Marine Resources and Coastal Engineering, Sun Yat-sen University. Helium and argon isotopic compositions of trapped hydrothermal fluids from the Yushui massive sulphide ores (including YS-035, YS-038, YS-040, YS-041, YS-042, and YS-044) were determined with an all-metal extraction line and a GV-5400 noble gas mass spectrometer

(GV Instruments, Manchester, UK) at the State Key Laboratory of Ore Deposit Geochemistry, Institute of Geochemistry, Chinese Academy of Sciences (Guiyang). For higher precision, another two samples (YS-008 and YS-020) were further analysed using a Thermo Fisher Helix Split-Flight-Tube (SFT) multi-collector mass spectrometer (Thermo Fisher Scientific, Waltham, MA, USA) at the Analytical Laboratory of Beijing Research Institute of Uranium Geology.

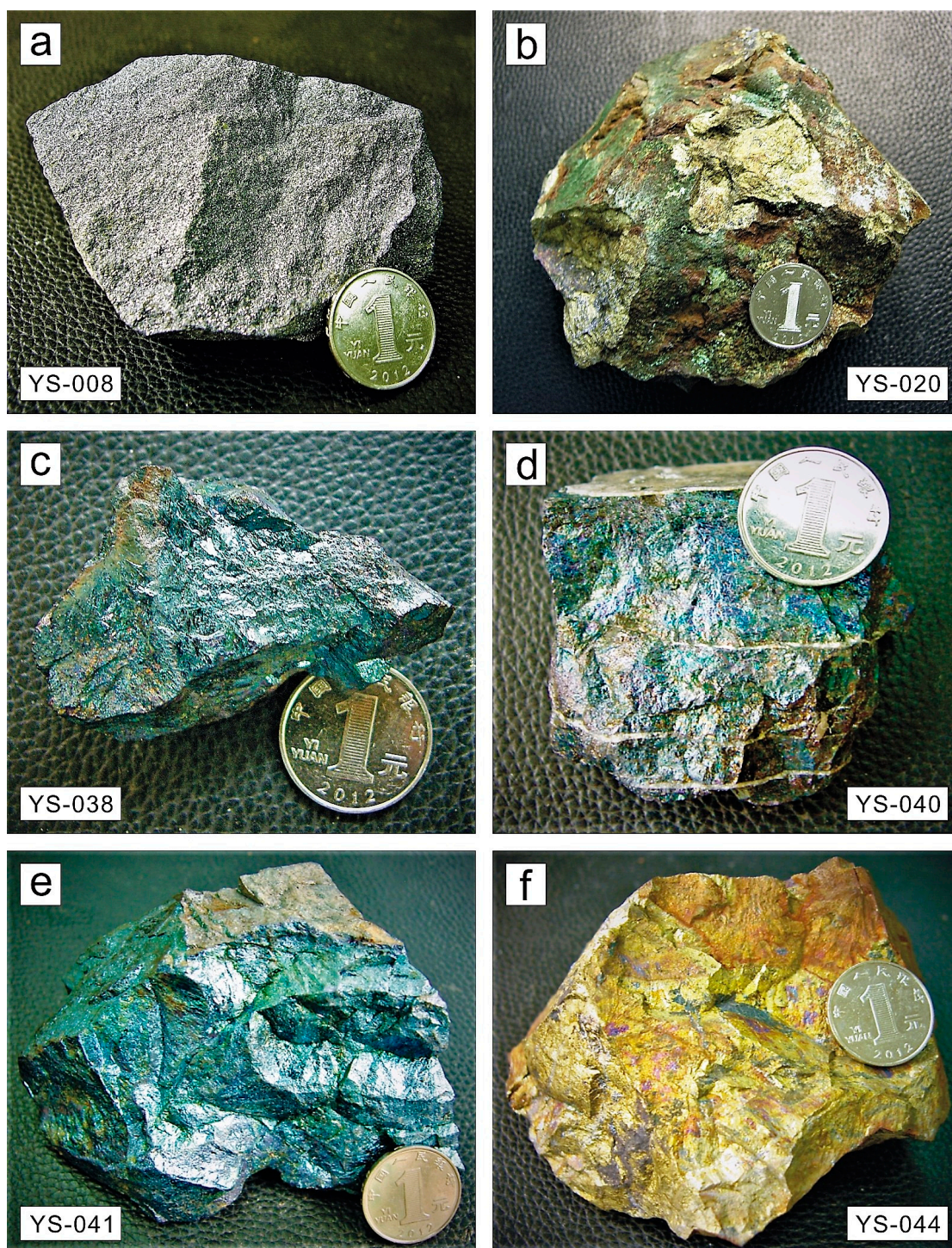


**Figure 3.** Photographs of selected hand specimens from the Yushui copper-polymetallic deposit. (a) Typical Pb-Zn-rich massive sulphide ore samples; (b–f) typical Cu-(Ag)-rich massive sulphide ore samples.

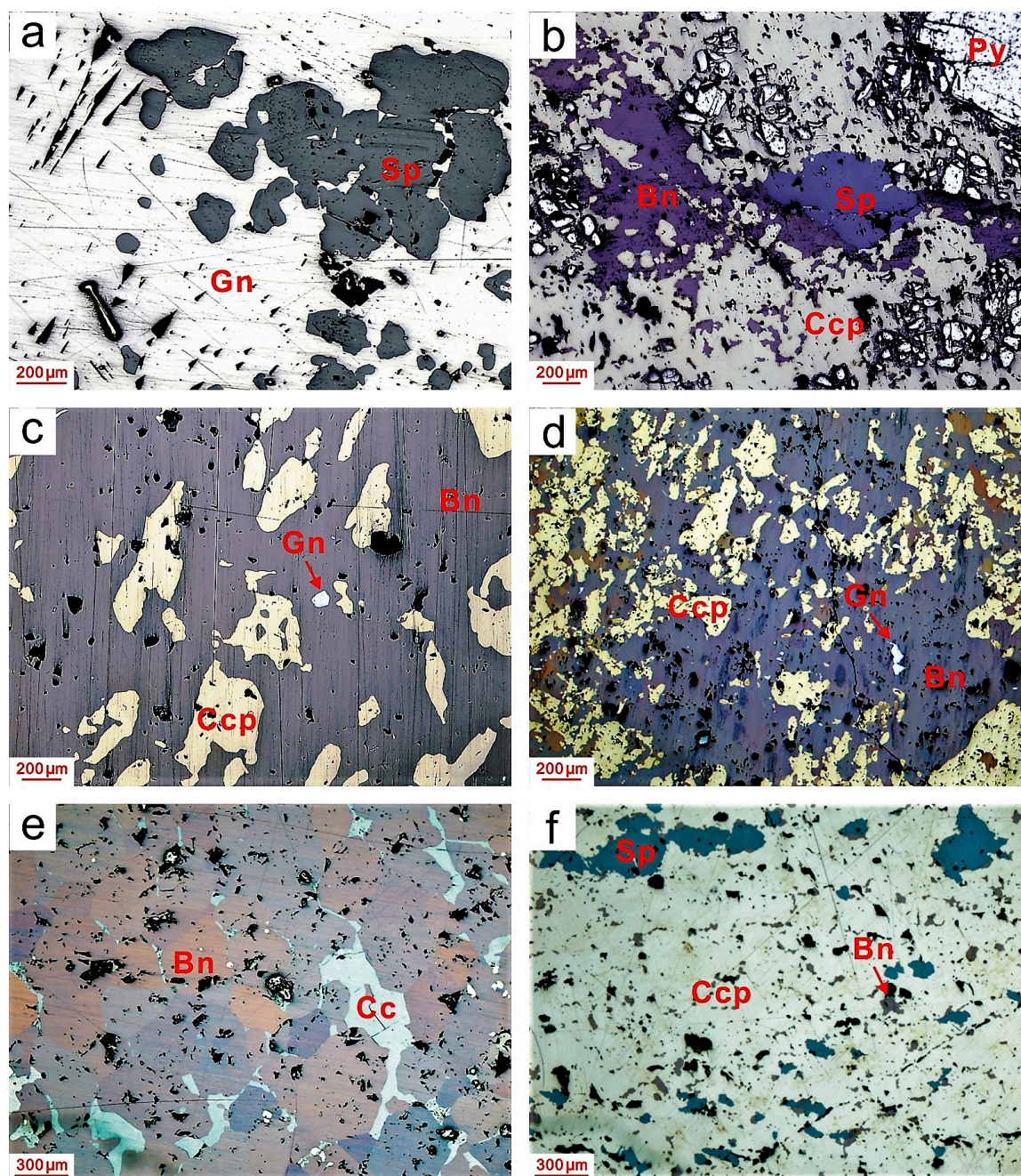


**Figure 4.** Representative reflected-light photomicrographs of selected polished thin sections from the Yushui copper-polymetallic deposit. (a) Colloform or irregular-shaped sphalerite aggregates occur as coarse-grained inclusions enclosed in massive porous galena (YS-008); (b) anhedral chalcopyrite aggregates coexisting with bornite, sphalerite and fine-grained pyrite (YS-020); (c,d) anhedral chalcopyrite crystals and trace amounts of galena or sulphosalts mostly occur as micro-inclusions disseminated in bornite matrix (YS-038 and YS-040); (e) anhedral to subhedral Ag-bearing chalcocite inclusions hosted in massive bornite aggregates (YS-041); (f) tiny bornite and sphalerite grains distributed in massive porous chalcopyrite matrix (YS-044). Mineral abbreviations: Bn = bornite, Cc = chalcocite, Ccp = chalcopyrite, Gn = galena, Py = pyrite, Sp = sphalerite.

Approximately 1 g of coarse-grained (generally 0.25–1.0 mm) hand-picked mineral separates were first cleaned ultrasonically several times in ethyl alcohol, then dried in vacuum and loaded in on-line crusher buckets. In order to facilitate complete removal of volatiles adsorbed on mineral surfaces or

trapped in subsurface voids, these samples were baked at  $\sim 150$  °C in an ultra-high vacuum system for >24 h prior to measurement. Fluid inclusion-hosted volatiles were released from mineral grains into the all-metal extraction system by sequential crushing in modified Nupro-type valves. The extracted gases were exposed to a titanium sponge furnace at 800 °C for 20 min to remove the bulk of active gases (such as CO<sub>2</sub> and H<sub>2</sub>O), and then exposed to two SAES Zr-Al getters (one at room temperature, the other at 450 °C) for 10 min to further purify. He was separated from Ar using an activated charcoal cold finger at liquid N<sub>2</sub> temperature ( $\sim 196$  °C) for 40–60 min to trap Ar, then He and Ar isotopes were analyzed using the GV-5400 or Helix SFT with relative errors of <10%. Noble gas abundances were measured by peak-height comparison with known amounts of standard air from an air bottle. Detailed sample preparation procedures and experimental methods used here were similar to those described in references [76–78]. The atmospheric <sup>3</sup>He/<sup>4</sup>He and <sup>40</sup>Ar/<sup>36</sup>Ar ratio is  $\sim 1.4 \times 10^{-6}$  and 295.5, respectively [79].

Analyses of (organic) trace gases trapped within fluid inclusions in this study were performed at the New Mexico Institute of Mining and Technology (NMT), USA. The cleaned and dried bornite or chalcopyrite samples ( $\sim 100$  mg each) were put into a swift crushing tube while being heated at about 100 °C and pumped at least 8 h (to eliminate secondary fluid inclusions), until a pressure lower than  $2 \times 10^{-7}$  Pa was attained in the gas extraction line. The ore mineral samples were crushed in a vacuum chamber housing the mass spectrometer (Balzers QMS-420, Balzers Instruments, Marin-Epagnier, Switzerland), and the released volatiles were quickly removed by the vacuum pumping system to a Balzers QMS-420 quadrupole mass spectrometer. The analytical precision is usually better than 5%. Most of the tubes for removing trace gases were made of glass, and the time for the removal was very short (less than 1 s), so that the released gases could keep their original compositions. The liquid-N<sub>2</sub>-condensable gases (including CO<sub>2</sub>, SO<sub>2</sub>, H<sub>2</sub>S, C<sub>2</sub>H<sub>4</sub>, C<sub>2</sub>H<sub>6</sub>, C<sub>3</sub>H<sub>6</sub>, C<sub>3</sub>H<sub>8</sub>, C<sub>4</sub>H<sub>8</sub>, C<sub>4</sub>H<sub>10</sub>, C<sub>6</sub>H<sub>6</sub>, and C<sub>7</sub>H<sub>8</sub>), non-condensable gases (e.g., H<sub>2</sub>, He, Ar, CH<sub>4</sub>, N<sub>2</sub>, and O<sub>2</sub>), and water are measured independently. The gas species are determined from an analog display of the mass spectra. Data processing was completed using the QUADSTAR-420 software (Version 3.0, Balzers Instruments, Marin-Epagnier, Switzerland). The experimental procedure was described in more details by previous researchers [48,62,63].

## 4. Results

### 4.1. He-Ar Concentrations and Isotopic Ratios

The measured abundances of fluid inclusion-hosted helium and argon in these massive sulphide samples vary over one to two orders of magnitude (as presented in Table 1, <sup>4</sup>He:  $2.27\text{--}160.00 \times 10^{-5}$  cm<sup>3</sup> STP g<sup>-1</sup>; <sup>3</sup>He:  $0.53\text{--}34.88 \times 10^{-12}$  cm<sup>3</sup> STP g<sup>-1</sup>; <sup>40</sup>Ar:  $6.28\text{--}37.82 \times 10^{-7}$  cm<sup>3</sup> STP g<sup>-1</sup>; <sup>36</sup>Ar:  $1.25\text{--}10.40 \times 10^{-9}$  cm<sup>3</sup> STP g<sup>-1</sup>). By comparison, only one chalcopyrite-rich massive sulphide sample (YS-020) collected from the  $-190$  m lower-level ore body contains the highest <sup>3</sup>He and <sup>4</sup>He concentrations among the remaining tested specimens, and significantly higher than those bornite-dominated samples from the  $-100$  m level ore body. On the contrary, most of the <sup>36</sup>Ar and <sup>40</sup>Ar contents in bornite aggregates from the richest Cu-bonanza ore body (except YS-041) are generally higher than in chalcopyrite or galena samples. Such variations in noble gas contents may also be attributed to differences in the actual size and population densities of fluid inclusions among various sulphide minerals, or even due to the variation in crushing/degassing efficiency (to a certain extent) [22,32]. Overall, these polymetallic sulphide ores exhibit a narrow range of <sup>3</sup>He/<sup>4</sup>He ratios from 0.006 to 0.056 R<sub>a</sub> ( $\sim 0.026$  R<sub>a</sub> on average, n = 8); while the <sup>40</sup>Ar/<sup>36</sup>Ar ratios range from 333.76 to 501.68, with an average of 397.53 which is greater than that of air-saturated water (ASW: 295.5) [79]. Moreover, a majority of the Yushui bornite samples have somewhat higher <sup>3</sup>He/<sup>4</sup>He ratios of trapped fluids ( $\sim 0.036$  R<sub>a</sub> on average) when compared to the chalcopyrite samples ( $\sim 0.011$  R<sub>a</sub> on average). Their calculated <sup>3</sup>He/<sup>4</sup>He ratios are considerably lower than the modern atmospheric end-member value, lying within the range of crustal reservoir [80].

**Table 1.** He-Ar concentrations ( $\text{cm}^3 \text{STP g}^{-1}$ ) and isotopic compositions of fluid inclusions hosted in massive sulphides from the Yushui ore deposit.

Sample No.	YS-035	YS-038	YS-040	YS-041	YS-042	YS-044	YS-008	YS-020
Minerals	Chalcopyrite	Bornite	Bornite	Bornite	Bornite	Chalcopyrite	Galena	Chalcopyrite
$^3\text{He}$ ( $10^{-12}$ )	$1.99 \pm 0.26$	$2.66 \pm 0.08$	$1.66 \pm 0.05$	$0.53 \pm 0.04$	$4.06 \pm 0.16$	$2.98 \pm 0.18$	2.01	34.88
$^4\text{He}$ ( $10^{-5}$ )	$22.41 \pm 0.34$	$3.43 \pm 0.05$	$4.27 \pm 0.07$	$2.27 \pm 0.03$	$7.07 \pm 0.11$	$20.80 \pm 0.32$	4.80	160.00
$^{40}\text{Ar}$ ( $10^{-7}$ )	$6.28 \pm 0.04$	$27.63 \pm 0.16$	$37.34 \pm 0.22$	$8.57 \pm 0.05$	$37.82 \pm 0.22$	$20.23 \pm 0.12$	13.96	12.96
$^{36}\text{Ar}$ ( $10^{-9}$ )	$1.25 \pm 0.03$	$8.25 \pm 0.06$	$10.40 \pm 0.06$	$1.97 \pm 0.03$	$8.82 \pm 0.12$	$6.06 \pm 0.07$	3.62	3.22
$^3\text{He}/^4\text{He}$ ( $R_a$ )	$0.006 \pm 0.001$	$0.056 \pm 0.002$	$0.028 \pm 0.001$	$0.017 \pm 0.001$	$0.041 \pm 0.002$	$0.010 \pm 0.001$	0.030	0.016
$^{40}\text{Ar}/^{36}\text{Ar}$	$501.68 \pm 12.32$	$334.87 \pm 3.02$	$359.06 \pm 3.06$	$434.28 \pm 7.88$	$428.62 \pm 6.23$	$333.76 \pm 4.12$	385.70	402.30
$^{40}\text{Ar}^*/^4\text{He}$	0.0012	0.0095	0.0155	0.0121	0.0166	0.0011	0.0068	0.0002
$F^4\text{He}$	1,081,365	25,149	24,793	69,407	48,398	207,394	80,149	3,000,697

Notes: 1. All errors are quoted at the  $1\sigma$  confidence level; 2. The unit for  $^3\text{He}$ ,  $^4\text{He}$ ,  $^{36}\text{Ar}$ , and  $^{40}\text{Ar}$  is  $\text{cm}^3 \text{STP g}^{-1}$ ; 3.  $^{40}\text{Ar}^* = ^{40}\text{Ar}_{\text{sample}} \times [1 - (^{40}\text{Ar}/^{36}\text{Ar})_{\text{atmosphere}} / (^{40}\text{Ar}/^{36}\text{Ar})_{\text{sample}}]$ ; 4.  $F^4\text{He}$  values reflect enrichment of  $^4\text{He}$  in the fluids relative to air,  $F^4\text{He} = (^4\text{He}/^{36}\text{Ar})_{\text{sample}} / (^4\text{He}/^{36}\text{Ar})_{\text{atmosphere}}$  where  $^4\text{He}/^{36}\text{Ar}_{\text{atmosphere}} = 0.1655$  [37]; 5. Except for two samples (No. YS-008 and YS-020) which were analyzed in the Analytical Laboratory of Beijing Research Institute of Uranium Geology, the other samples were measured in the State Key Laboratory of Ore Deposit Geochemistry, Institute of Geochemistry, Chinese Academy of Sciences (Guiyang).

#### 4.2. Trace Gas Analysis of Fluid Inclusions

Inclusion volatiles were measured in bornite and chalcopyrite from the −100 m level of No. 2 stope (main ore bodies) in the Yushui deposit. The abundances of trace gases (such as He, Ar, and N<sub>2</sub>) in fluid inclusions are presented in Table 2. It appears that the analytical variation in the same crushed sample is quite small. In addition to the determination of conservative gas species N<sub>2</sub>, Ar, and He in ore-forming fluids, the concentrations and ratios of organic gases were also measured for comparison. Bulk analytical results of fluid inclusions in the Yushui massive sulphide ores are shown in Table 3. These volatile organic compounds are mainly composed of CH<sub>4</sub> and CO<sub>2</sub>, together with C<sub>2</sub>–C<sub>7</sub> (i.e., C<sub>2</sub>H<sub>4</sub>, C<sub>2</sub>H<sub>6</sub>, C<sub>3</sub>H<sub>6</sub>, C<sub>3</sub>H<sub>8</sub>, C<sub>4</sub>H<sub>8</sub>, C<sub>4</sub>H<sub>10</sub>, C<sub>6</sub>H<sub>6</sub>, and C<sub>7</sub>H<sub>8</sub>). Other than methane, the most abundant hydrocarbons are ethane (C<sub>2</sub>H<sub>6</sub>), propane (C<sub>3</sub>H<sub>8</sub>), n-butane (C<sub>4</sub>H<sub>10</sub>), propylene (C<sub>3</sub>H<sub>6</sub>) and butane (C<sub>4</sub>H<sub>10</sub>). Minor amounts of ethylene (C<sub>2</sub>H<sub>4</sub>), butene (C<sub>4</sub>H<sub>8</sub>), benzene (C<sub>6</sub>H<sub>6</sub>), and toluene (C<sub>7</sub>H<sub>8</sub>) were also detected (except for one chalcopyrite sample). By contrast, the concentrations of hydrocarbons larger than C<sub>4</sub> were very low, thus can be regarded as negligible. Furthermore, the final freezing temperature and initial melting temperature of CO<sub>2</sub> inclusions were somewhat lower than the standard values, suggesting the existence of other trace gases. However, not all of the organic species recorded in mass spectra have been identified and calibrated due to the limitations of testing methods. Hence, the amount of condensable organic compounds has been calculated to date by assuming all are CH<sub>4</sub> and C<sub>2</sub>–C<sub>7</sub> light hydrocarbons [48].

**Table 2.** N<sub>2</sub>, Ar and He contents (mol. %) in sulphide-hosted fluid inclusions from the Yushui deposit.

Mineral	Description	Crush No.	N <sub>2</sub>	Ar	He	N <sub>2</sub> /Ar	Ar/He
bornite	Hand-picked separates of fine-grained aggregates from the Cu bonanza ores	1	0.3782	0.0014	0.0461	270.1	0.030
		2	0.0405	<0.0001	0.0054	-	-
		3	0.0302	<0.0001	0.0098	-	-
		4	0.4806	0.0048	0.0519	100.1	0.092
		5	0.0280	<0.0001	0.0087	-	-
		6	0.0395	0.0001	0.0065	395.0	0.015
chalcopyrite	Hand-picked separates of fine-grained aggregates from massive sulphide ores	1	1.4548	0.0003	0.0164	4849.3	0.018
		2	0.9537	0.0003	0.0088	3179.0	0.034
		3	0.8076	0.0003	0.0073	2692.0	0.041
		4	1.9852	0.0007	0.0237	2836.0	0.030
		5	0.4037	0.0004	0.0127	1009.3	0.031
		6	0.1917	0.0004	0.0084	479.3	0.048
		7	0.2421	0.0003	0.0096	807.0	0.031
		8	0.1415	0.0003	0.0084	471.7	0.036
		9	0.0797	0.0003	0.0078	265.7	0.038

**Table 3.** Light hydrocarbons and CO<sub>2</sub> contents (mol. %) in sulphide-hosted fluid inclusions from the Yushui Cu-rich ore samples.

Sampling Location	Selected from Some of the Richest Bonanza Ore Bodies at the −100 m Level of No. 2 Stope in the Yushui Copper-Polymetallic Deposit						Selected from Typical Stratiform Massive Sulphide Ore Bodies at the −100 m Level of No. 2 Stope in the Yushui Deposit					
	Hand-Picked Separates of Fine-Grained Bornite Aggregates						Hand-Picked Separates of Fine-Grained Chalcopyrite Aggregates					
Crush No.	1	2	3	4	5	6	1	2	3	4	5	6
CH <sub>4</sub>	55.31	38.85	47.53	63.43	47.42	38.91	1.204	1.638	1.073	1.259	1.266	0.968
C <sub>2</sub> H <sub>4</sub>	0.292	0.211	0.218	0.288	<0.001	<0.001	<0.001	<0.001	<0.001	<0.001	<0.001	<0.001
C <sub>2</sub> H <sub>6</sub>	1.049	0.497	0.786	1.275	0.870	1.114	0.093	0.101	0.090	0.093	0.092	0.082
C <sub>3</sub> H <sub>6</sub>	0.104	0.064	0.104	0.066	0.057	0.041	0.064	0.063	0.062	0.062	0.065	0.052
C <sub>3</sub> H <sub>8</sub>	0.750	0.451	0.619	0.787	0.330	0.441	0.142	0.150	0.132	0.138	0.150	0.128
C <sub>4</sub> H <sub>8</sub>	0.209	0.062	0.128	0.275	0.026	0.086	0.003	0.005	0.005	0.004	0.003	0.004
C <sub>4</sub> H <sub>10</sub>	0.341	0.094	0.218	0.467	0.033	0.109	0.002	0.002	0.003	0.003	0.002	0.003
C <sub>6</sub> H <sub>6</sub>	0.142	0.065	0.105	0.164	0.014	0.010	0.001	0.001	0.001	0.001	0.001	0.001
C <sub>7</sub> H <sub>8</sub>	0.032	0.009	0.020	0.049	0.001	0.002	<0.001	<0.001	<0.001	<0.001	<0.001	<0.001
CO <sub>2</sub>	41.77	59.70	50.27	33.20	51.25	59.29	98.49	98.04	98.64	98.44	98.42	98.76
CO <sub>2</sub> /CH <sub>4</sub>	0.76	1.54	1.06	0.52	1.08	1.52	81.78	59.86	91.92	78.21	77.73	102.00
CH <sub>4</sub> /C <sub>2</sub> H <sub>6</sub>	52.72	78.23	60.46	49.75	54.48	34.92	12.99	16.23	11.98	13.52	13.76	11.81
C <sub>2</sub> H <sub>6</sub> /C <sub>3</sub> H <sub>8</sub>	1.40	1.10	1.27	1.62	2.64	2.52	0.65	0.67	0.68	0.67	0.61	0.64

## 5. Discussion

### 5.1. Helium and Argon Sources

According to previously published results of noble gas isotopes, helium and argon trapped in fluid inclusions generally originate from three main sources: (1) air-saturated water (ASW, including meteoric fluids and groundwater), which is characterized by atmospheric He and Ar isotopic compositions ( $^3\text{He}/^4\text{He} = 1R_a$ ,  $^{40}\text{Ar}/^{36}\text{Ar} = 295.5$ ) [79]; (2) mantle magmatic volatiles, which are produced from most mantle-derived rocks including the oceanic lithosphere characterized by a well-defined  $^3\text{He}/^4\text{He}$  ratio of  $1\text{--}1.3 \times 10^{-5}$  ( $7\text{--}9 R_a$ ), while mantle-derived Ar is dominated by radiogenic  $^{40}\text{Ar}$  with  $^{40}\text{Ar}/^{36}\text{Ar} > 40,000$  [81–83]; (3) fluids of crustal origin, including formation water or sedimentary basin brines. It has been suggested that high concentrations of large-ion lithophile elements (LILEs, such as U, Th and K) in the continental crust can produce abundant radiogenic/nucleogenic Ar and He, with  $^{40}\text{Ar}/^{36}\text{Ar}$  ratios  $\geq 45,000$  and  $^3\text{He}/^4\text{He}$  ratios  $\leq 0.1 R_a$ , respectively [80]. In this study, our data indicate that He–Ar isotopic compositions of the Yushui sulphide samples are relatively close to each other ( $^3\text{He}/^4\text{He}$ : 0.006–0.056  $R_a$ ;  $^{40}\text{Ar}/^{36}\text{Ar}$ : 333.76–501.68). All these  $^3\text{He}/^4\text{He}$  and  $^{40}\text{Ar}/^{36}\text{Ar}$  ratios are well consistent with the range of crust-originated fluids (0.01–0.05  $R_a$ ), suggestive of crustal components as the predominant source of noble gases, with little or no contribution from mantle-derived fluids (Figure 5). The proportional contribution of atmospheric He to the ore-forming fluids can also be estimated by calculation of the  $F^4\text{He}$  value (i.e., the ratio of  $^4\text{He}/^{36}\text{Ar}$  in the sample to the atmospheric  $^4\text{He}/^{36}\text{Ar} \sim 0.1655$ ). Overall, the calculated  $F^4\text{He}$  values of the Yushui ore deposit are greater than 24,000 (Table 1). In other words, the  $^4\text{He}$  content in each sulphide sample was more than 24,000 times that of the atmosphere, implying that seawater and/or meteoric water might play a negligible role in copper-polymetallic mineralization.

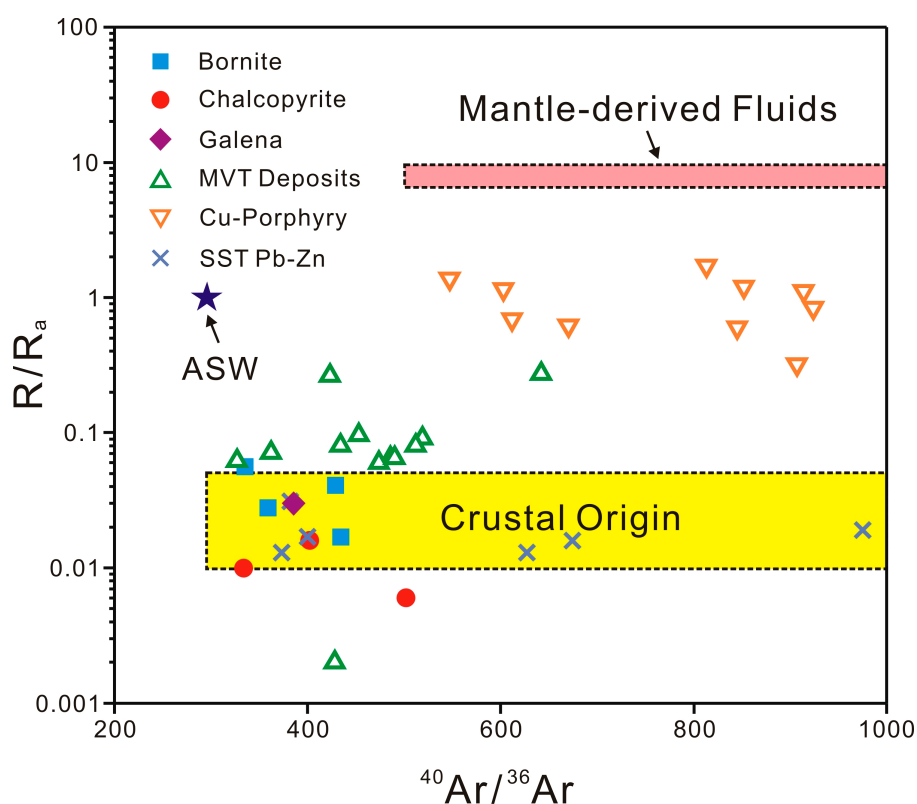


**Figure 5.**  $^{40}\text{Ar}/^{36}\text{Ar}$  versus  $R/R_a$  diagram of fluid inclusions hosted within massive sulphide samples from the Yushui Cu-polymetallic ore deposit. Plots of data points from representative Porphyry-Cu ore systems, Mississippi Valley-type (MVT) and sandstone-type (SST) Pb-Zn deposits are also shown for comparison, given by [37–40].

In addition, the  $^{40}\text{Ar}^*/^4\text{He}$  values of our studied samples vary from 0.0011 to 0.0166, while the  $^{40}\text{Ar}^*/^4\text{He}$  value of crustal source (present-day average crustal production ratio) is approximately 0.2 [80]. In contrast, the mantle beneath the crust has a higher  $^{40}\text{Ar}^*/^4\text{He}$  value of  $\sim 0.5$  (where  $^{40}\text{Ar}^*$  is the non-atmospheric  $^{40}\text{Ar}$  contribution) [28,29,80,84]. Notably, a majority of these data plotted in the  $^{40}\text{Ar}^*/^4\text{He}$ - $R/R_a$  diagram (Figure 6) are lower than the  $^{40}\text{Ar}^*/^4\text{He}$  value of crustal fluids. According to previous researchers, the  $^{40}\text{Ar}^*/^4\text{He}$  value of modern groundwater may decrease when groundwater flows through regional rocks, as  $^4\text{He}$  is preferentially leached and mobilized in comparison with  $^{40}\text{Ar}$  [85]. Actually, the concentrations of radiogenic  $^{40}\text{Ar}$  and  $^4\text{He}$  in groundwater (derived from crustal rocks) are related to the closure temperatures of Ar and He. For most minerals, the closure temperature of He is less than  $200\text{ }^\circ\text{C}$ , while the closure temperature of  $^{40}\text{Ar}$  is usually higher than  $200\text{ }^\circ\text{C}$ . According to previous microthermometric results obtained from the Yushui ore deposit, the homogenization temperatures of fluid inclusions mainly ranged from  $110\text{ }^\circ\text{C}$  to  $220\text{ }^\circ\text{C}$  [12], indicating that  $^4\text{He}$  was preferentially partitioned into the metal-bearing solutions. Therefore, the relatively low values of  $^{40}\text{Ar}^*/^4\text{He}$  for the Yushui ore-forming fluids may be resulted from the remobilization and redistribution of highly radioactive  $^4\text{He}$  from the strata during continuous leaching/hydrothermal reworking processes.

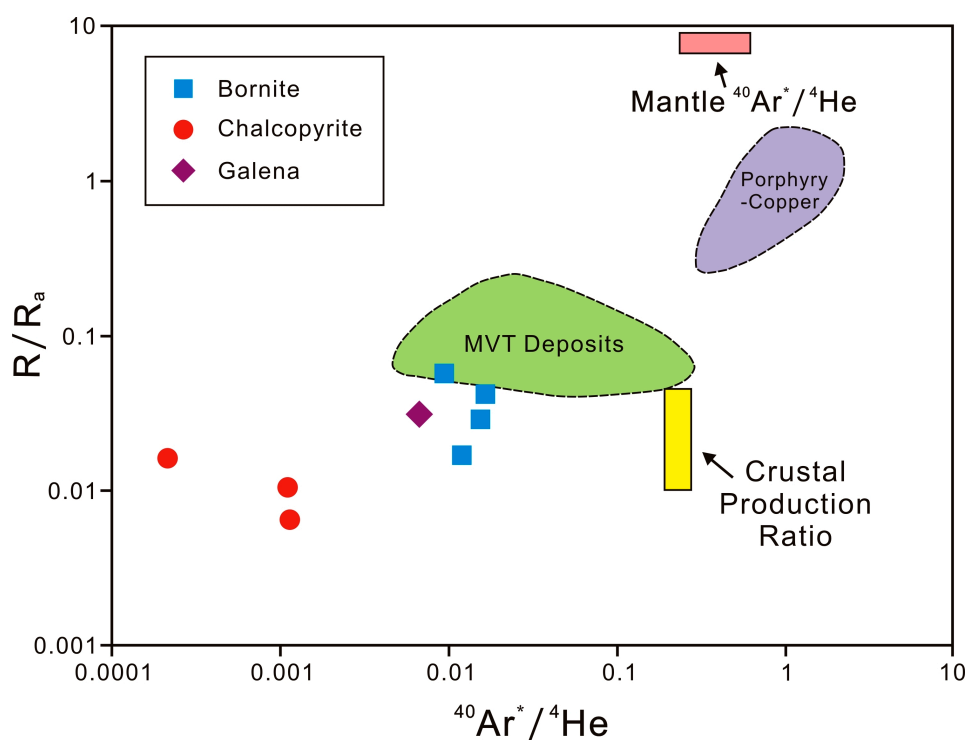


**Figure 6.**  $^{40}\text{Ar}^*/^4\text{He}$  versus  $R/R_a$  diagram of fluid inclusions hosted within massive sulphide samples from the Yushui Cu-polymetallic ore deposit (modified after [84]). Data sources from the previously published literature [37–39] and this study.

As shown in Figure 6, the  $^{40}\text{Ar}^*/^4\text{He}$  ratios of chalcopyrite samples (No. YS-020, YS-035, and YS-044) were much lower than those of bornite and galena samples. Likewise, the  $^3\text{He}/^4\text{He}$  ratios of these three samples were also slightly lower than the other five samples. In fact, bulk chemical analyses of trace-element compositions (unpublished data) reveal that the concentrations of large-ion lithophile elements (especially U and REEs) in selected chalcopyrite-rich samples were significantly higher than those in the other bornite-rich ores, and the radiogenic  $^4\text{He}$  produced from radioactive decay of uranium may have increased the contents of  $^4\text{He}$  in these U-rich samples and thus led to a decrease of the  $^{40}\text{Ar}^*/^4\text{He}$  ratios. On the other hand, extremely high contents of total REEs in such chalcopyrite samples ( $\Sigma\text{REE}$  up to  $>20,000$  ppm) are positively correlated with the enrichment of U (Figure 7), indicating that these elements were probably accumulated in the same period and controlled by similar geological factors. Based on

the preliminary results of geochemical analyses and optical microscopic observations, we suggest that some of the Yushui ore bodies might be locally affected by late-stage hydrothermal reworking and alteration. As a result, those sulphide samples with elevated U and REE concentrations have yielded somewhat anomalous He-Ar isotopic ratios in their fluid inclusions. Nevertheless, the other Cu-rich bonanza samples from the Yushui main ore bodies were not superimposed by strong metamorphic overprinting (only weakly affected). Therefore, these results may represent the initial He-Ar isotope compositions of ore-forming fluids. The mixture of crustal reservoir can impart distinct He-Ar isotopic signatures to the hydrothermal products during Cu-mineralization processes in the Yushui deposit, as demonstrated by the lowest  $F^4\text{He}$  values measured in those bornite-rich samples with relatively higher  $^{40}\text{Ar}^*/^4\text{He}$  ratios close to that of the crustal production ( $\sim 0.2$ ) [84].

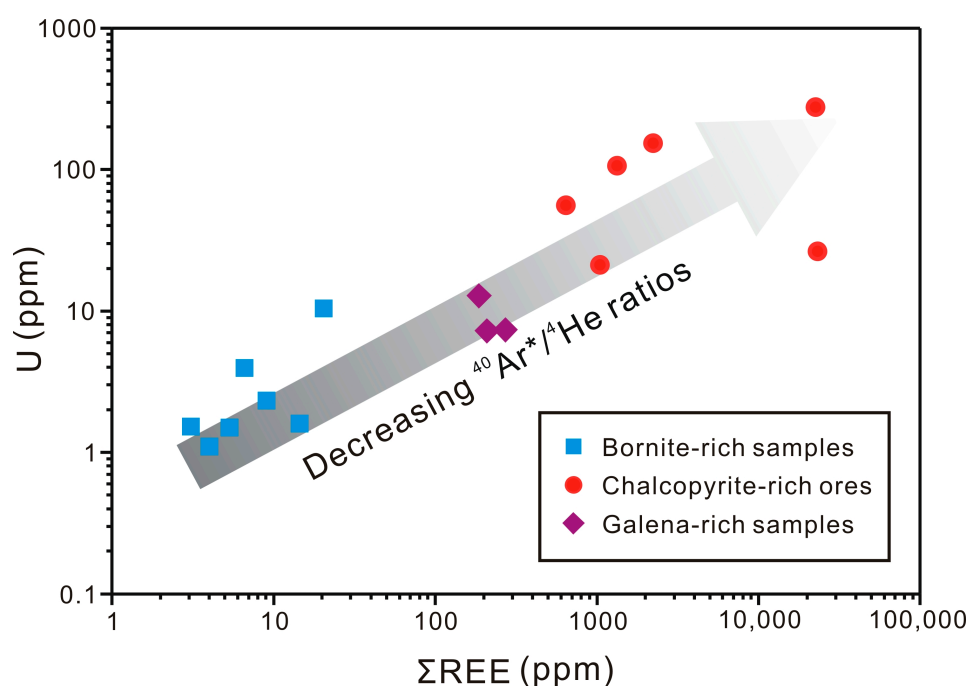


**Figure 7.** Scatter plots of total rare earth elements (REEs) versus U concentrations (ppm) in different types of the Yushui sulphide samples. Note that there is a strong positive correlation between these two elements, along with the variation trend of decreasing  $^{40}\text{Ar}^*/^4\text{He}$  ratios during copper-polymetallic mineralisation.

### 5.2. The $\text{N}_2$ -Ar-He Systematics

Some authors have proposed that the compositions of trace gases (such as  $\text{N}_2$ , Ar, and He) in geothermal systems can be used to determine the ratios among magmatic water, crustal fluids and meteoric water in hydrothermal solutions [56–58]. As shown in the  $\text{N}_2/100$ -Ar-He  $\times 10$  (NAH) ternary diagram (Figure 8), the trace gas ratios associated with distinct sources/reservoirs are markedly different. The basic principle is as follows: the  $\text{N}_2/\text{Ar}$  ratio in the modern atmosphere is around 83.6, but the  $\text{N}_2/\text{Ar}$  ratio of ASW (including seawater) is somewhat lower ( $\sim 38$ ) since the solubility of Ar in water is higher than that of  $\text{N}_2$ . The meteoric water is plotted near label Ar in Figure 8 because it is enriched in Ar. During plate subduction, a large amount of marine sediments were carried to the deep crust. Decomposition of organic matters in subducted sediments might have released a large amount of  $\text{N}_2$ , which makes the mantle-derived magmatic water plotted near label  $\text{N}_2/100$  in Figure 8 (Zone A), with  $\text{N}_2/\text{Ar}$  ratios higher than 200 because of its richness in  $\text{N}_2$ . As mentioned above, helium (especially  $^4\text{He}$ ) is mostly derived from the decay of radioactive elements. Due to high contents of U and Th in the continental crust, crustal water (enriched in helium) is plotted near label He $\times 10$  (Zone B). It has also been suggested that the magmatic water from rift basalts or rhyolites partly overlaps the

field of crustal water in this NAH diagram (Zone C), but their corresponding different  $^3\text{He}/^4\text{He}$  ratios could be used to distinguish them [51,52,54,56–58].

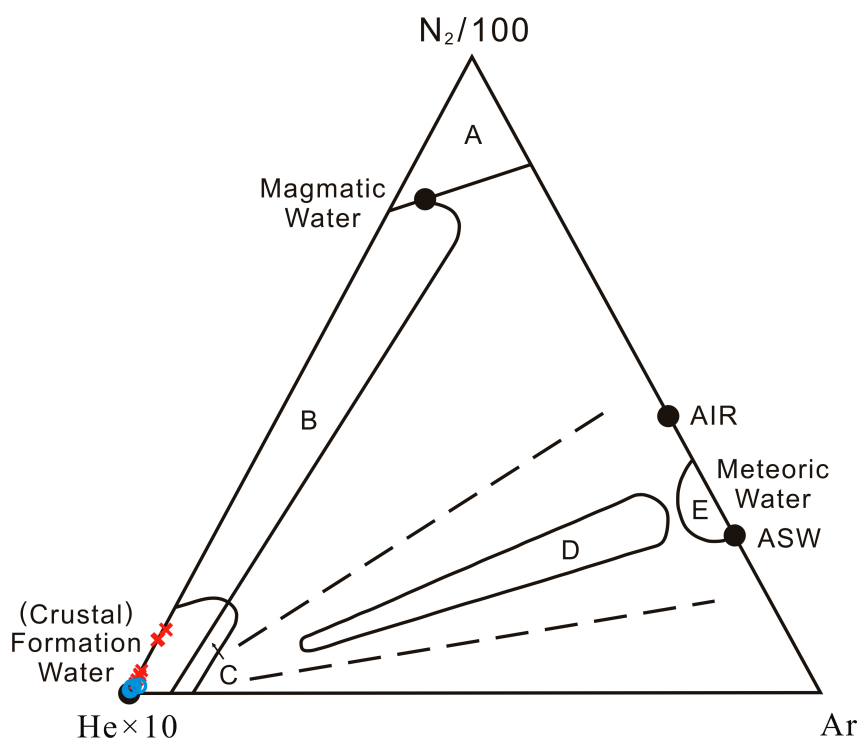


**Figure 8.**  $\text{N}_2/100\text{-Ar-He} \times 10$  ternary diagram of ore-forming fluids in the Yushui deposit (modified after [49]). Zone A: magmatic water; Zone B: formation water (sedimentary brines); Zone C: fluid from rift basalt/rhyolite; Zone D: deep-circulating meteoric water; Zone E: shallow-circulating meteoric water, including seawater/air saturated water (ASW). “x”: chalcopyrite samples; “o”: bornite samples from the bonanza ore body.

The compositions of trace gases in sulphide inclusions of the Yushui copper-polymetallic deposit are listed in Table 2. The results of  $\text{N}_2$ , Ar, and He in replicate samples were in good agreement, with a small range of variability. This may suggest that the analytical method is reliable, and the (trapped) gas/fluid ratios are quite stable in fluid inclusions. Hence, boiling is not the major mechanism for metal deposition, which may cause great variation of gas/fluid ratios [49,51]. In the NAH diagram, we find that most of the analytical data are plotted in Zone B and Zone C, representing the source ranges of formation water (sedimentary hot brines) and/or fluids from rift-related basalt/rhyolite, respectively. Combined with the He-Ar isotopic tracers, we can rule out the possibility that the ore-forming fluids were derived from ASW/meteoric water and/or deep magmatic water associated with continental rift basalt/rhyolite. Obviously, the  $\text{N}_2\text{-Ar-He}$  systematics are generally consistent with previous integrated studies of He-Ar isotopes, thus can provide more geochemical evidence to support the crustal origin of Yushui ore-forming fluids (mainly derived from formation water/basinal brines). However, it should be noted that several chalcopyrite samples show a systematic increase in  $\text{He}/\text{N}_2$  ratios towards magmatic end-member value, possibly suggestive of an insignificant mixing trend between crustal and mantle components during fluid evolution and hydrothermal alteration processes.

### 5.3. Compositions of Light Hydrocarbon Gases

Ore-forming fluids of sediment-hosted, stratabound massive sulphide deposits, especially formation water or sedimentary basinal brines, usually contain a large amount of organic matters. The organic matters are principally composed of light hydrocarbon gases because most of liquid hydrocarbons are unstable at (medium to high) ore-forming temperatures [60]. It has been proposed that light hydrocarbons in crustal fluids were mainly generated by thermal cracking

of kerogens caused by interactions between crustal fluids and organic matters in sedimentary rocks [57–59]. Here, two end-member components have been recognized in these light hydrocarbon gases. One component (called the “natural gas type” for short) was generated in the interaction of crustal fluids with sedimentary rocks at medium-low temperatures. Its composition is predominantly made up of a sequence of saturated hydrocarbon species decreasing steadily from  $\text{CH}_4$  to higher saturated alkanes. The ratios of  $\text{CH}_4/\text{C}_2\text{H}_6$  and  $\text{C}_2\text{H}_6/\text{C}_3\text{H}_8$  are about 50–350 and 2.5, respectively; while the contents of unsaturated olefins and aromatic hydrocarbons are very low. Such features are very similar to those of natural gases. The other component (called the “magmatic volatile type” for short) was produced by fluid–rock interactions at high temperatures ( $>400\text{ }^\circ\text{C}$ ) during magmatic intrusion, consisting essentially of  $\text{CH}_4$  with rapidly decreasing contents of higher species of saturated alkanes. The ratios of  $\text{CH}_4/\text{C}_2\text{H}_6$  and  $\text{C}_2\text{H}_6/\text{C}_3\text{H}_8$  are higher than 1000 and about 10, respectively, along with (easily measurable) high concentrations of unsaturated alkenes and aromatic hydrocarbons. The reason for this is that high-temperature conditions favor the formation of short-chain alkanes and unsaturated alkenes [57,59,62,63].

As presented in Table 3, the  $\text{CH}_4/\text{C}_2\text{H}_6$  ratios for the Yushui ore-forming fluids are about 10–80, while the  $\text{C}_2\text{H}_6/\text{C}_3\text{H}_8$  ratios are mostly less than 3. In addition, the concentrations of unsaturated alkenes/olefins and aromatic hydrocarbons are very low. Thus, the light hydrocarbon organic gases in our tested specimens obviously belong to the so-called “natural gas type”. The results in Figure 9 also demonstrate that almost all of these analytical data are plotted in the field of “natural gas type”, implying that the light hydrocarbon gases in ore-forming fluids of the Yushui deposit (especially for Ag-rich bornite samples) were probably generated by thermal cracking of kerogens caused by fluid–rock interactions at medium-low temperatures. On the other hand, an increase in  $\text{CO}_2/\text{CH}_4$  ratios is generally correlated with decreasing  $^{40}\text{Ar}^*/^{4}\text{He}$  values in fluid inclusions (following the paragenetic sequence from bornite to chalcopyrite, accompanied by progressive low-grade regional metamorphism). Nevertheless, the main-stage Cu–Ag mineralization processes (which had occurred before the Yanshanian magmatism) seem not to have been strongly affected by later-stage, high-temperature magmatic activities. In fact, the intrusion of Mesozoic diabase dykes or granitoids in the mining area might not have a direct relationship with the Yushui main ore bodies. This geological phenomenon is also consistent with our conclusions.

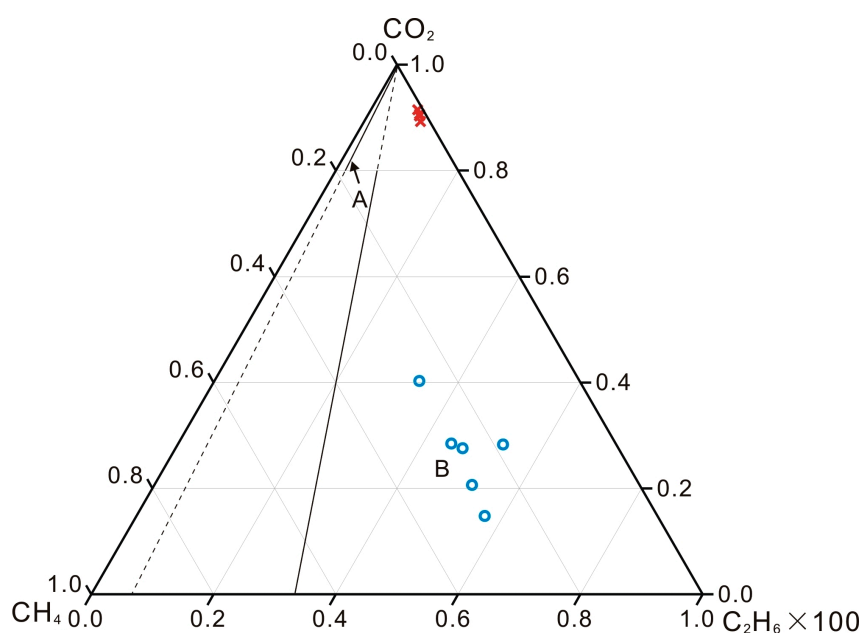


**Figure 9.**  $\text{CH}_4\text{-CO}_2\text{-C}_2\text{H}_6 \times 100$  ternary diagram of fluid inclusions in massive sulphides from the Yushui copper polymetallic ore deposit (modified after the published literature [55,57,62]). A: “magmatic/metamorphic volatile type” field; B: “natural gas type” field; “x”: chalcopyrite samples; “o”: bornite samples from the Cu-rich bonanza ore body.

However, it must be emphasized that this classification diagram for the  $\text{CO}_2\text{-CH}_4\text{-C}_2\text{H}_6$  ternary system could only be established/used semi-quantitatively. Thermodynamic modelling indicates that fluid inclusions containing  $\text{CO}_2$  and significant amounts of  $\text{CH}_4$  will re-equilibrate and precipitate graphite during cooling, thus resulting in post-entrapment compositional changes [86]. Noteworthily, the dashed lines in Figure 9 only roughly mark the ambiguous boundaries of “evolved magmatic” or “composite fluid” fields. Generally speaking, the typical volatiles associated with magmatic activity are characterized by  $\text{CO}_2$  and only minor  $\text{CH}_4$  [53,66]. Although the characteristic carbon-bearing volcanic vapor is considered to be  $\text{CO}_2$ , reports on the presence of hydrocarbons in igneous rocks (formed by abiogenic processes) have actually increased in recent years. Most of the occurrences are due to the incorporation of organic materials into the magmatic systems [87]. For example, fluid inclusions in minerals from alkaline igneous complexes contain distinctly different carbon-bearing volatiles, which are dominated by hydrocarbon-rich gases (essentially  $\text{CH}_4$ ) with only insignificant amounts of  $\text{CO}_2$  [88]. Therefore, these hydrocarbons may not be as rare as previously thought. Moreover, the domain “A” also covers almost all the field of metamorphic fluids, and thus may not always represent magmatic volatiles or volcanic vapors in its totality. In some cases, evolved meteoric waters, metamorphic or deep-sea hydrothermal vent fluids with elevated  $\text{CO}_2/\text{CH}_4$  ratios may also be plotted in the upper part of this ternary diagram (close to label  $\text{CO}_2$ ) [89–91]. So it is necessary to combine the composition of organic gases in fluid inclusions with the  $\text{N}_2\text{-Ar-He}$  tracing systematics. Here, we introduce a  $\text{CO}_2/\text{CH}_4$  vs.  $\text{N}_2/\text{Ar}$  diagram to unambiguously identify fluid sources [92]. Overall, the  $\text{CO}_2/\text{CH}_4$  ratios of crustal fluids are usually below 4 [53,66]. Note that the variation range of bornite samples in Figure 10 generally falls within the domain of organic-rich formation waters. As for chalcopyrite samples, data presented in Table 2 give  $\text{N}_2/\text{Ar}$  ratios in the general range of ~266 to 4849, whereas corresponding  $\text{CO}_2/\text{CH}_4$  ratios vary from ~60 to 102. Most of these analytical results plotted outside the crustal box (near or within the domain of composite fluid, see Figure 10) are obviously distinct from those of bornite-rich samples ( $\text{N}_2/\text{Ar}$ : ~100–395;  $\text{CO}_2/\text{CH}_4$ : 0.52–1.54), and thus can be explained in terms of mixing between magmatic fluids and a crustal component (i.e., formation waters/basinal brines), but only to a limited degree.

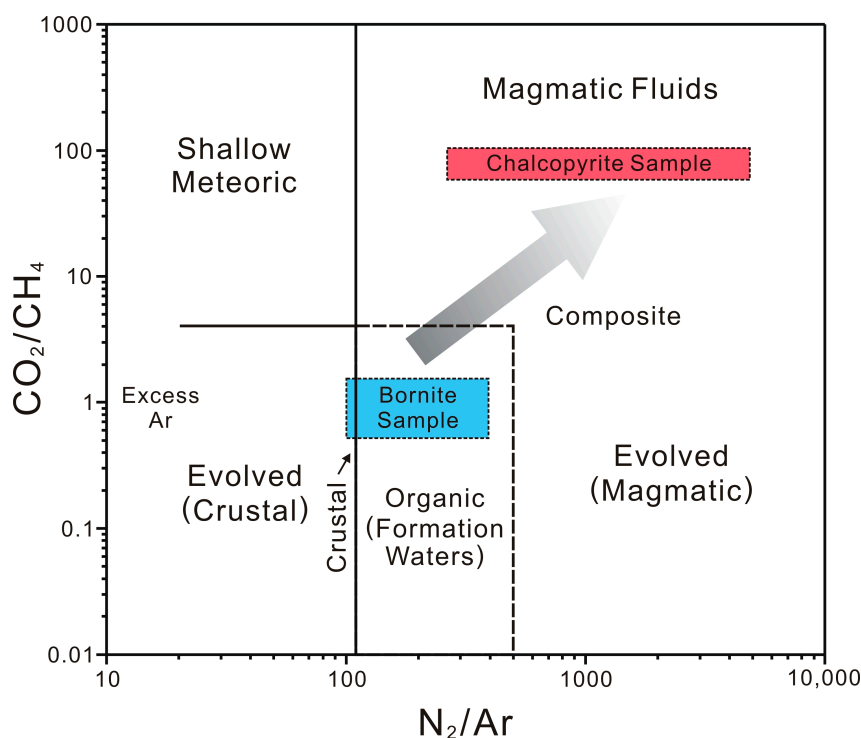


**Figure 10.** Compilation of  $\text{CO}_2/\text{CH}_4$  versus  $\text{N}_2/\text{Ar}$  data for Cu-rich sulphides from the Yushui ore deposit (modified after the published literature [55,66,92]).

#### 5.4. Possible Mechanisms for the Oxidation of Hydrocarbons to CO<sub>2</sub>

Besides chalcopyrite, a recent study [12] also reveals the presence of abundant CO<sub>2</sub>-rich fluid inclusions, together with aqueous inclusions in both opaque and transparent minerals (including sphalerite, quartz, and calcite) from the Yushui ore deposit. In contrast to the hydrocarbon-rich fluid inclusions within bornite samples, it should be noted that such CO<sub>2</sub>-rich fluids are uncharacteristic of basinal brines, but somewhat comparable to those of orogenic or magmatic mineralization systems [90,91]. Typically, hydrocarbon fluids are important parts of basinal hydrothermal settings. Sulphur speciation and concentrations in deep basinal brines play a crucial role in the formation of many sediment-hosted polymetallic sulphide deposits [93]. In particular, one of the most important reactions controlling the sulphur behavior in deep sedimentary environments is the abiogenic reduction of sulphate to sulphide (occurring at temperature above 100–140 °C) coupled with the oxidation of hydrocarbons, which is termed thermochemical sulphate reduction (TSR) [94–96]. Thus, the TSR process involving hydrocarbons may contribute significantly to the genesis of both MVT and SEDEX ore deposits [97–99]. Moreover, it has been suggested that siliceous limestones commonly experience insignificant decarbonation/decomposition of carbonates under contact metamorphic conditions; whereas for most sedimentary rocks enriched in organic matter, CH<sub>4</sub> rather than CO<sub>2</sub> will be released [100]. Therefore, infiltration of external, hot fluids into the host strata might increase the CH<sub>4</sub> generation from devolatilization reactions (or partially by removal of organic carbon from the host rocks). However, this is clearly not the case with the Yushui fluids trapped in chalcopyrite.

To explain this, we propose that late-stage hydrothermal alteration caused by oxidized ore-bearing solutions that penetrated into the Caledonian basement might result in an oxidation effect of soluble organic gases and materials (i.e., methane or other light hydrocarbons), which is manifested by elevated CO<sub>2</sub>/CH<sub>4</sub> ratios and secondary enrichment of U-REE in most chalcopyrite-rich samples (Figure 7), as well as a decrease in the content of saturated hydrocarbons (see Table 3). Theoretically, methane can be oxidized to carbon dioxide (CH<sub>4</sub> + 2O<sub>2</sub> = CO<sub>2</sub> + 2H<sub>2</sub>O) via two distinct geological processes: (1) AOM reaction (anaerobic oxidation of methane) mediated by sulphate-reducing bacteria in an anoxic environment, and (2) TOM (thermochemical oxidation of methane) at relatively high temperatures by sulphate or high-valence metal oxides. Both processes typically result in the formation of authigenic carbonate. Although it is difficult to distinguish between thermochemical and bacterial sulphate reduction (BSR) in sediment-hosted base metal deposits, S-isotope ratios of sulphide products and fluid inclusion data can be used as distinguishing criteria, and provide geochemical evidence for identification of a bacterial versus a thermochemical origin [95,96]. Previously, we have already investigated the sulphur isotopic signatures of various ore minerals to infer the sources of paleo-hydrothermal fluids. Unpublished isotopic data produced by bulk analyses of hand-picked mineral separates show a narrow range of δ<sup>34</sup>S values varying from −4.9 to 1.5 per mil (δ<sup>34</sup>S<sub>Bornite</sub>: −4.9–−0.5‰V-CDT, with an average of −3.4‰; δ<sup>34</sup>S<sub>Chalcopyrite</sub>: −4.3–−1.2‰V-CDT, with an average of −3.1‰; δ<sup>34</sup>S<sub>Galena</sub>: −2.7–−1.7‰V-CDT, with an average of −2.2‰; δ<sup>34</sup>S<sub>Pyrite</sub>: −3.1–−1.5‰V-CDT, with an average of −0.6‰). All these results are comparable to the majority of typical SEDEX and MVT deposits, where the reduced sulphur was interpreted to be mainly derived from TSR [95,96].

Moreover, organic gas reservoirs in sedimentary basins are generally buried to depths of several kilometers experiencing temperatures from 60 to 150 °C [101], while the metabolism of archaea/sulphate-reducing bacteria responsible for AOM are mainly active at temperatures below 80 °C (i.e., dominating the conversion of CH<sub>4</sub> to CO<sub>2</sub> only under limited conditions). During prograde metamorphism, methane directly formed by cracking of higher hydrocarbons under elevated temperature will become increasingly enriched in <sup>13</sup>C as a result [102]. Although there are no carbon-isotope data available for the CH<sub>4</sub> or carbonate (e.g., calcite/dolomite cements) associated with the Yushui ore bodies, anaerobic oxidation of methane by bacteria or archaea can also be ruled out on the basis of our microthermometric measurements, because the estimated homogenization temperatures (about 120–190 °C) of fluid inclusions in sphalerite and transparent minerals from the main metallogenic stage would have been too high for sulphate-reducing bacteria to survive [96].

Furthermore, mixing and contamination by oxidised methane during the extraction is also considered unlikely because of the rapidity of sample handling and experimental procedures. Hence, TSR is potentially the predominant mechanism for hydrocarbon oxidation in the strata with high formation temperature (especially  $> 80\text{ }^{\circ}\text{C}$ ). Recently, geological evidence has been reported for the oxidation of  $\text{CH}_4$  induced by high-valence metal oxides or by  $\text{Fe}^{3+}$  in detrital biotite (chloritization) at temperatures above  $270\text{ }^{\circ}\text{C}$  during metamorphism [101,103,104], but this needs to be further confirmed. In sum, methane in early-formed Cu-rich sulphide assemblages was mainly derived from cracking of the precursor hydrocarbons. At increasing metamorphic conditions under more oxidizing conditions, an unusual depletion of methane in main-stage high-temperature chalcopyrite samples can be explained by the oxidation of hydrocarbons to  $\text{CO}_2$  and  $\text{H}_2\text{O}$ . This is supported by the contemporaneous increase of  $\text{CO}_2$  contents in the trapped volatiles (locally produced by TSR during the later hydrothermal reworking and alteration).

### 5.5. Constraints on the Genesis of Yushui Ore Deposit

It can be concluded that the compositions of fluid inclusions in most Cu-rich sulphide samples may represent fluid features of the principal ore-forming stage. Analyses of their He-Ar isotopic ratios and trace gas characteristics indicate that main sources of the Yushui ore-forming fluids were derived from basinal hot brines (crustal formation water) in the host strata rather than magmatic input or shallow-/deep-circulating seawater, even though fluids for the Nanling metallogenic belt are generally considered to have been sourced (substantially) from seawater by convection [1]. Previous studies have suggested that cations dissolved in the liquid phase of fluid inclusions hosted by the main-stage ore-mineral assemblages (such as bornite and chalcopyrite) are predominantly composed of  $\text{Ca}^{2+}$  and  $\text{Na}^+$ , followed by  $\text{K}^+$  and  $\text{Mg}^{2+}$ ; while the identified anion species were mainly  $\text{SO}_4^{2-}$  and  $\text{Cl}^-$ , followed by  $\text{F}^-$ . The  $\text{Na}^+/\text{K}^+$  ratios ranged from 1.29 to 30.78, and the  $\text{F}^-/\text{Cl}^-$  ratios varied from 0.016 to 1 [8]. It is generally thought that the  $\text{Na}^+/\text{K}^+$  ratio in magmatic hydrothermal fluids is less than 1, and greater than 1 in metamorphic or pegmatite deposits; whereas higher values will be observed in ore-forming fluids associated with sedimentary rocks or underground hot brines [105]. Some authors also found that magmatic hydrothermal fluids are commonly rich in  $\text{F}^-$ , while hydrothermal fluids (such as underground hot brines from primary sedimentary basins) have low  $\text{F}^-/\text{Cl}^-$  ratios (usually less than 1) [106]. Therefore, the  $\text{Na}^+/\text{K}^+$  and  $\text{F}^-/\text{Cl}^-$  ratios in the liquid phase of sulphide inclusions [8] also indicate that ore-forming fluids of the Yushui copper-polymetallic deposit should be derived from sedimentary hot brines (formation water), but have little genetic relationship with the later stage magmatism and/or relevant hydrothermal event (except for a number of chalcopyrite samples).

Disputable direct dating of the bornite-dominated assemblage has been recently discussed in the literature. Our isotopic data yielded a Re-Os isochron age of  $308 \pm 15\text{ Ma}$ , which is interpreted to represent the age of ore deposition for these Cu-rich massive sulphides [11]. Thus, the formation of the Yushui ore bodies, especially the main stage of Cu-Ag mineralization, is coeval with the host rocks. Previously published results reported an initial  $^{187}\text{Os}/^{188}\text{Os}$  ratio of  $1.81 \pm 0.34$  for the Yushui polymetallic sulphide deposit, with the  $\gamma_{\text{Os}}(t)$  value up to +1349, suggesting a major contribution of crustal materials to ore-forming processes [11]. According to ore-bearing properties in this district [107], high concentrations of copper, lead, zinc and silver were detected in the surrounding strata formed in the Predevonian era (the Caledonian basement), which might provide an important source of ore-forming materials. Combined with the geological features of the Yushui deposit, it is proposed that the mining area was affected by the Hercynian tectonic activities, resulting in regional extension. This event led to an increase in the geothermal gradient within this area, which might have produced basinal hot brines/formation water in the Caledonian tectonic layer. Abundant ore-forming elements were also leached and transported by the fluids over the same period. Subsequently, paleo-hydrothermal fluids migrated along the deep dilational faults, carried the metals upwards, and formed the massive sulphide ore bodies. The penetration-circulation of basinal brines (deep downward) into the basement

rocks may be a main driving mechanism for extraction of base metals and silver [108]. In summary, the Yushui copper-polymetallic deposit may be of sedimentary exhalative origin.

## 6. Conclusions

(1) The  $^3\text{He}/^4\text{He}$  ratios (0.006–0.056  $R_a$ ) and  $^{40}\text{Ar}/^{36}\text{Ar}$  values (333.76–501.68) of fluid inclusions in massive sulphides from the Yushui copper-polymetallic deposit are well within the range of crustal reservoir, thus indicating that the main-stage Cu-rich solutions may be predominantly derived from crustal fluids without the mixing of mantle fluids or seawater. To a lesser extent, the ore-forming fluids may have inherited the radiogenic He isotopic signatures from the surrounding strata. As a result, the  $^{40}\text{Ar}^*/^4\text{He}$  values of most chalcopyrite samples were generally lower than those of bornite-rich samples, suggesting that the main ore bodies might be locally influenced by later stage hydrothermal reworking and alteration.

(2) Combined with He-Ar isotopic tracers, the compositions of trace gases ( $\text{N}_2$ -Ar-He systematics) in Ag-rich bornite crystals also indicate that such metal-bearing solutions probably originated from formation water (basinal hot brines), rather than magmatic water or circulating meteoric water. In addition, a variety of light hydrocarbon species identified in the Yushui fluid inclusions provide additional constraints on the origin of ore-forming fluids.

(3) The organic gases in the ore-forming fluids of the Yushui deposit are mainly composed of  $\text{C}_1$ – $\text{C}_4$  alkanes, while the contents of unsaturated olefins and aromatic hydrocarbons were very low, indicating that the processes of copper-polymetallic mineralization were not directly affected by high-temperature magmatism. As hydrothermal alteration proceeded,  $\text{CO}_2$  and  $\text{H}_2\text{O}$  trapped within fluid inclusions may have formed by the breakdown and oxidation of organic matter.

**Author Contributions:** Y.H. and X.S. conceived and designed the experiments; Y.H. and Z.W. analyzed the data and wrote this paper; Z.W., X.S., and W.Z. have substantially revised the original manuscript; G.S. and Y.H. provided great support for sampling during our field work; Y.W. contributed materials/analysis tools; Y.H., Z.W., and Y.G. also made significant contributions to the sample preparation.

**Funding:** This research project was jointly supported by the National Natural Science Foundation of China (Grant No. 41602092, 41702066, 41503036 and 41273054), Open Research Fund Program of Guangdong Provincial Key Laboratory of Marine Resources and Coastal Engineering (No. 201505 and GDKLMRCE1805), Open Fund of Key Laboratory of Marine Mineral Resources, Ministry of Land and Resources (No. KLMMR-2015-B-04), Guangdong Province Universities and Colleges Pearl River Scholar Funded Scheme (2011), the Fundamental Research Funds for Central Universities (No. 12lgjc05), and the China Ocean Mineral Resources Research and Development Association (DYXM-115-02-1-11).

**Acknowledgments:** We thank Guohao Jiang from Institute of Geochemistry, Chinese Academy of Sciences (Guiyang) and Hanbin Liu at the Analytical Laboratory of Beijing Research Institute of Uranium Geology for their assistance with He-Ar analyses. We particularly want to pay tribute to David Norman, a well-respected and distinguished geologist who dedicated his whole life to the research career of ore-forming fluid geochemistry. The corresponding author also gratefully acknowledges Andrew Campbell and Beverly Chomiak for their technical help during his visit in NMT. Last but not least, the authors sincerely appreciate for the editors' warm help and great patience, as well as three anonymous reviewers' thoughtful comments and constructive suggestions.

**Conflicts of Interest:** The authors declare no conflict of interest.

## References

1. Gu, L.; Zaw, K.; Hu, W.; Zhang, K.; Ni, P.; He, J.; Xu, Y.; Lu, J.; Lin, C. Distinctive features of Late Palaeozoic massive sulphide deposits in South China. *Ore Geol. Rev.* **2007**, *31*, 107–138. [[CrossRef](#)]
2. He, Y. Metallogenic-geologic characteristics of Yushui hydrothermal-sedimentary polymetallic deposit in Meixian County, Guangdong Province. *Guangdong Geol.* **1990**, *5*, 1–13. (In Chinese)
3. Chen, B.; Chen, J.; Guo, R.; Yu, S. The genesis of Yushui copper-polymetallic deposit in Meixian County, Guangdong Province. *Guangdong Geol.* **1992**, *7*, 59–69. (In Chinese)
4. He, Y. Geology of Yushui copper-lead-zinc (silver) deposit, Meixian. *Guangdong Geol.* **1997**, *12*, 41–48. (In Chinese)

5. Wang, L.; Yang, M.; Peng, S. On the genesis of the Yushui polymetallic deposit in Meixian County, Guangdong Province. *Geotecton. Metall.* **1999**, *23*, 345–352. (In Chinese)
6. Chen, H. A study on the isotopic geochemical exploration in the Yushui-Yinshi copper and polymetallic mineralization belt, Guangdong. *Acta Geosci. Sin.* **1994**, *15*, 152–156. (In Chinese)
7. Cai, J.; Liu, J.; Chen, Y.; Qiu, Q. Metallogenetic epoch of Yushui copper polymetallic deposit of Meixian, Guangdong. *Guangdong Geol.* **1996**, *11*, 55–58. (In Chinese)
8. Liu, J. Thermobarogeochemistry, ore-forming age and genesis study for the Yushui copper-rich multimetal deposit in Meixian County, Guangdong Province, southern China. *Geol. Miner. Resour. South China* **1997**, *1*, 37–50. (In Chinese)
9. Guo, R.; Chen, B.; Yu, S. Mineralogy of the Yushui Cu-polymetallic deposit in Meixian, Guangdong. *Geol. Explor. Nonferrous Met.* **1999**, *8*, 428–431. (In Chinese)
10. Chen, W. The ore-forming geology condition and origin of Yushui copper-polymetallic deposit. *Nonferrous Met.* **2007**, *59*, 18–19. (In Chinese)
11. Huang, Y.; Sun, X.; Shi, G.; Sa, R.; Guan, Y.; Jiang, X.; Que, H. Re-Os dating of sulphides from the Yushui Cu-polymetallic deposit in eastern Guangdong Province, South China. *Ore Geol. Rev.* **2015**, *70*, 281–289. [[CrossRef](#)]
12. Jiang, B.; Zhu, X.; Cheng, X.; Wang, H. Characteristics and geological significance of fluid inclusions in the Yushui copper polymetallic deposit, Guangdong Province. *Geol. China* **2016**, *43*, 2163–2172. (In Chinese)
13. He, Y. Silver in Yushui copper-lead-zinc deposit, Meixian. *Guangdong Geol.* **1997**, *12*, 33–36. (In Chinese)
14. Liu, X. Copper resources in China: Today and tomorrow. *Northwest. Geol.* **2007**, *40*, 83–88. (In Chinese)
15. Gu, L.; Hu, W.; Ni, P.; He, J.; Xu, Y.; Lu, J.; Lin, C.; Li, W. New discussion on the South China-type massive sulphide deposits formed on continental crust. *Geol. J. China Univ.* **2003**, *9*, 592–608. (In Chinese)
16. Lupton, J.E.; Craig, H. A major helium-3 source at 15°S on the East Pacific Rise. *Science* **1981**, *214*, 13–18. [[CrossRef](#)] [[PubMed](#)]
17. Simmons, S.F.; Sawkins, F.J.; Schlutter, D.J. Mantle-derived helium in two Peruvian hydrothermal ore deposits. *Nature* **1987**, *329*, 429–432. [[CrossRef](#)]
18. Lupton, J.E.; Baker, E.T.; Massoth, G.J. Variable <sup>3</sup>He/heat ratios in submarine hydrothermal systems: Evidence from two plumes over the Juan de Fuca ridge. *Nature* **1989**, *337*, 161–164. [[CrossRef](#)]
19. Baker, E.T.; Lupton, J.E. Changes in submarine hydrothermal <sup>3</sup>He/heat ratios as an indicator of magmatic/tectonic activity. *Nature* **1990**, *346*, 556–558. [[CrossRef](#)]
20. Stuart, F.M.; Turner, G.; Duckworth, R.C.; Fallick, A.E. Helium isotopes as tracers of trapped hydrothermal fluids in ocean-floor sulfides. *Geology* **1994**, *22*, 823–826. [[CrossRef](#)]
21. Stuart, F.M.; Burnard, P.G.; Taylor, R.P.; Turner, G. Resolving mantle and crustal contributions to ancient hydrothermal fluids: He-Ar isotopes in fluid inclusions from Dae Hwa W-Mo mineralization, South Korea. *Geochim. Cosmochim. Acta* **1995**, *59*, 4663–4673. [[CrossRef](#)]
22. Jean-Baptiste, P.; Fouquet, Y. Abundance and isotopic composition of helium in hydrothermal sulfides from the East Pacific Rise at 13°N. *Geochim. Cosmochim. Acta* **1996**, *60*, 87–93. [[CrossRef](#)]
23. Hu, R.; Burnard, P.G.; Turner, G.; Bi, X. Helium and argon isotope systematics in fluid inclusions of Machangqing copper deposit in west Yunnan Province, China. *Chem. Geol.* **1998**, *146*, 55–63. [[CrossRef](#)]
24. Burnard, P.G.; Hu, R.; Turner, G.; Bi, X. Mantle, crustal and atmospheric noble gases in Ailaoshan gold deposits, Yunnan Province, China. *Geochim. Cosmochim. Acta* **1999**, *63*, 1595–1604. [[CrossRef](#)]
25. Hou, Z.; Li, Y.; Ai, Y.; Tang, S.; Zhang, Q. Helium isotopic compositions of the active hydrothermal system in the Okinawa trough: Evidence for the mantle-derived helium. *Sci. China Ser. D Earth Sci.* **1999**, *29*, 155–162. (In Chinese)
26. Winckler, G.; Aeschbach-Hertig, W.; Kipfer, R.; Botz, R.; Rübél, A.P.; Bayer, R.; Stoffers, P. Constraint on origin and evolution of Red Sea brines from helium and argon isotopes. *Earth Planet. Sci. Lett.* **2001**, *184*, 671–683. [[CrossRef](#)]
27. Zeng, Z.; Qin, Y.; Zhai, S. He, Ne and Ar isotope compositions of fluid inclusions in hydrothermal sulfides from the TAG hydrothermal field, Mid-Atlantic Ridge. *Sci. China Ser. D Earth Sci.* **2001**, *44*, 221–228. [[CrossRef](#)]
28. Ballentine, C.J.; Burnard, P.G. Production, release and transport of noble gases in the continental crust. *Rev. Mineral. Geochem.* **2002**, *47*, 481–538. [[CrossRef](#)]

29. Graham, D.W. Noble gas isotope geochemistry of Mid-Ocean Ridge and Ocean Island Basalts: Characterization of mantle source reservoirs. *Rev. Mineral. Geochem.* **2002**, *47*, 247–317. [[CrossRef](#)]
30. Hou, Z.; Zaw, K.; Li, Y.; Zhang, Q.; Zeng, Z.; Tetsuro, U. Contribution of magmatic fluid to the active hydrothermal system in the JADE field, Okinawa Trough: Evidence from fluid inclusions, oxygen and helium isotopes. *Int. Geol. Rev.* **2005**, *47*, 420–437.
31. Lüders, V.; Niedermann, S. Helium isotope composition of fluid inclusions hosted in massive sulfides from modern submarine hydrothermal systems. *Econ. Geol.* **2010**, *105*, 443–449. [[CrossRef](#)]
32. Zeng, Z.; Niedermann, S.; Chen, S.; Wang, X.; Li, Z. Noble gases in sulfide deposits of modern deep-sea hydrothermal systems: Implications for heat fluxes and hydrothermal fluid processes. *Chem. Geol.* **2015**, *409*, 1–11. [[CrossRef](#)]
33. Guan, Y.; Ren, Y.; Sun, X.; Xiao, Z.; Guo, Z. Helium and argon isotopes in the Fe-Mn polymetallic crusts and nodules from the South China Sea: Constraints on their genetic sources and origins. *Minerals* **2018**, *8*, 471. [[CrossRef](#)]
34. Wang, Y.; Wu, Z.; Sun, X.; Deng, X.; Guan, Y.; Xu, L.; Huang, Y.; Cao, K. He-Ar-S isotopic compositions of polymetallic sulphides from hydrothermal vent fields along the ultraslow-spreading Southwest Indian Ridge and their geological implications. *Minerals* **2018**, *8*, 512. [[CrossRef](#)]
35. Stuart, F.M.; Turner, G. The abundance and isotopic composition of the noble gases in ancient fluids. *Chem. Geol.* **1992**, *101*, 97–109. [[CrossRef](#)]
36. Hu, R.; Turner, G.; Burnard, P.G.; Zhong, H.; Ye, Z.; Bi, X. Helium and argon isotopic geochemistry of Jinding superlarge Pb-Zn deposit. *Sci. China Ser. D Earth Sci.* **1998**, *41*, 442–448. [[CrossRef](#)]
37. Kendrick, M.A.; Burgess, R.; Patrick, R.A.D.; Turner, G. Fluid inclusion noble gas and halogen evidence on the origin of Cu-Porphyry mineralising fluids. *Geochim. Cosmochim. Acta* **2001**, *65*, 2651–2668. [[CrossRef](#)]
38. Kendrick, M.A.; Burgess, R.; Leach, D.; Patrick, R.A.D. Hydrothermal fluid origins in Mississippi valley-type ore districts: combined noble gas (He, Ar, Kr) and halogen (Cl, Br, I) analysis of fluid inclusions from the Illinois-Kentucky fluorspar district, Viburnum Trend, and Tri-State districts, midcontinent United States. *Econ. Geol.* **2002**, *97*, 453–469.
39. Kendrick, M.A.; Burgess, R.; Patrick, R.A.D.; Turner, G. Hydrothermal fluid origins in a fluorite-rich Mississippi valley-type district: combined noble gas (He, Ar, Kr) and halogen (Cl, Br, I) analysis of fluid inclusions from the South Pennine ore field, United Kingdom. *Econ. Geol.* **2002**, *97*, 435–451. [[CrossRef](#)]
40. Kendrick, M.A.; Burgess, R.; Harrison, D.; Bjørlykke, A. Noble gas and halogen evidence for the origin of Scandinavian sandstone-hosted Pb-Zn deposits. *Geochim. Cosmochim. Acta* **2005**, *69*, 109–129. [[CrossRef](#)]
41. Zhao, K.; Jiang, S.; Xiao, H.; Ni, P. Origin of ore-forming fluids of the Dachang Sn-polymetallic ore deposit: Evidence from helium isotopes. *Chin. Sci. Bull.* **2002**, *47*, 1041–1045. [[CrossRef](#)]
42. Xue, C.; Chen, Y.; Wang, D.; Yang, J.; Yang, W.; Zeng, R. Geology and isotopic composition of helium, neon, xenon and metallogenic age of the Jinding and Baiyangping ore deposits, northwest Yunnan, China. *Sci. China Ser. D Earth Sci.* **2003**, *46*, 789–800. [[CrossRef](#)]
43. Hu, R.; Burnard, P.G.; Bi, X.; Zhou, M.; Peng, J.; Su, W.; Wu, K. Helium and argon isotope geochemistry of alkaline intrusion-associated gold and copper deposits along the Red River-Jinshajiang fault belt, SW China. *Chem. Geol.* **2004**, *203*, 305–317. [[CrossRef](#)]
44. Sun, X.; Wang, M.; Xue, T.; Ma, M.; Li, Y. He-Ar isotopic systematics of fluid inclusions in pyrites from PGE-polymetallic deposits in Lower Cambrian black rock series, South China. *Acta Geol. Sin.* **2004**, *78*, 471–475.
45. Sun, X.; Zhang, Y.; Xiong, D.; Sun, W.; Shi, G.; Zhai, W.; Wang, S. Crust and mantle contributions to gold-forming process at the Daping deposit, Ailaoshan gold belt, Yunnan, China. *Ore Geol. Rev.* **2009**, *36*, 235–249. [[CrossRef](#)]
46. Zhai, W.; Sun, X.; Wu, Y.; Sun, Y.; Hua, R.; Ye, X. He-Ar isotope geochemistry of the Yaoling-Meiziwo tungsten deposit, North Guangdong Province: Constraints on Yanshanian crust-mantle interaction and metallogenesis in SE China. *Chin. Sci. Bull.* **2012**, *57*, 1150–1159. [[CrossRef](#)]
47. Yang, F.; Li, Q.; Yang, C.; Zhang, Z. A combined fluid inclusion and S-H-O-He-Ar isotope study of the Devonian Ashele VMS-type copper-zinc deposit in the Altay orogenic belt, northwest China. *J. Asian Earth Sci.* **2018**, *161*, 139–163. [[CrossRef](#)]
48. Norman, D.I.; Sawkins, I.J. Analysis of volatiles in fluid inclusions by mass spectrometer. *Chem. Geol.* **1987**, *61*, 1–10. [[CrossRef](#)]
49. Norman, D.I.; Musgrave, J.A. N<sub>2</sub>-Ar-He compositions in fluid inclusions: Indicators of fluid source. *Geochim. Cosmochim. Acta* **1994**, *58*, 1119–1131. [[CrossRef](#)]

50. Graney, J.R.; Kesler, S.E. Factors affecting gas analysis of inclusion fluid by quadrupole mass spectrometry. *Geochim. Cosmochim. Acta* **1995**, *59*, 3977–3986. [[CrossRef](#)]
51. Sun, X.; Norman, D.I.; Sun, K.; Chen, B.; Chen, J. N<sub>2</sub>-Ar-He systematics and source of ore-forming fluid in Changkeng Au-Ag deposit, central Guangdong, China. *Sci. China Ser. D Earth Sci.* **1999**, *42*, 475–481. [[CrossRef](#)]
52. Sun, X.; Norman, D.I.; Sun, K.; Chen, J.; Chen, B. A new indicator of ore-forming fluid sources: N<sub>2</sub>-Ar-He compositions in fluid inclusions. *Geol. Rev.* **2000**, *46*, 99–104. (In Chinese)
53. Moore, J.N.; Norman, D.I.; Kennedy, B.M. Fluid inclusion gas compositions from an active magmatic-hydrothermal system: A case study of the Geysers geothermal field, USA. *Chem. Geol.* **2001**, *173*, 3–30. [[CrossRef](#)]
54. Sun, X.; Norman, D.I.; Sun, K.; Chen, J.; Chen, B. N<sub>2</sub>-Ar-He tracing systematics of ore-forming fluids: A case study from the Songxi large-scale Ag (Sb) deposit, eastern Guangdong Province, China. *Prog. Nat. Sci.* **1999**, *9*, 1364–1367. (In Chinese)
55. Sun, X.; Wang, M.; Xue, T.; Sun, K. New advances in research of trace gaseous compositions in fluid inclusions and their applications as indicators of ore-forming fluid sources and processes. *Earth Sci. Front.* **2004**, *11*, 471–478. (In Chinese)
56. Giggenbach, W.F.; Sano, Y.; Wakita, H. Isotopic composition of helium, and CO<sub>2</sub> and CH<sub>4</sub> contents in gases produced along the New Zealand part of a convergent plate boundary. *Geochim. Cosmochim. Acta* **1993**, *57*, 3427–3455. [[CrossRef](#)]
57. Giggenbach, W.F.; Sheppard, D.S.; Robinson, B.W.; Stewart, M.K.; Lyon, G.L. Geochemical structure and position of the Waiotapu geothermal field, New Zealand. *Geothermics* **1994**, *23*, 599–644. [[CrossRef](#)]
58. Giggenbach, W.F. Variations in the chemical and isotopic composition of fluids discharged from the Taupo Volcanic Zone, New Zealand. *J. Volcanol. Geotherm. Res.* **1995**, *68*, 89–116. [[CrossRef](#)]
59. Giggenbach, W.F. Relative importance of thermodynamic and kinetic processes in governing the chemical and isotopic composition of carbon gases in high-heatflow sedimentary basins. *Geochim. Cosmochim. Acta* **1997**, *61*, 3763–3785. [[CrossRef](#)]
60. Zhuang, H.; Lu, J.; Fu, J.; Liu, J.; Shi, J. Preliminary study on light hydrocarbons in ore-forming fluids of gold and antimony deposits in southwestern Guizhou, China. *Chin. Sci. Bull.* **1997**, *42*, 1708–1711. [[CrossRef](#)]
61. Sun, X.; Norman, D.I.; Sun, K.; Chen, B.; Chen, J. Compositions of light hydrocarbons in fluid inclusions and its significance for ore genesis—A case study of Songxi Ag (Sb) deposit, eastern Guangdong. *Geol. Rev.* **1999**, *45*, 817–821. (In Chinese)
62. Sun, X.; Norman, D.I.; Sun, K.; Chen, B.; Chen, J. Organic gases in fluid inclusions of ore minerals and their constraints on ore genesis: A case study of the Changkeng Au-Ag deposit, Guangdong, China. *Acta Geol. Sin.* **2003**, *77*, 86–94.
63. Sun, X.; Norman, D.I.; Sun, K.; Wang, M.; Chen, B.; Chen, J.; Yu, S. Light hydrocarbons in fluid inclusions and their constraints on ore genesis: A case study of the Songxi Ag (Sb) deposit, Eastern Guangdong, China. *Acta Geol. Sin.* **2003**, *77*, 227–236.
64. Kendrick, M.A.; Honda, M.; Oliver, N.H.S.; Phillips, D. The noble gas systematics of late-orogenic H<sub>2</sub>O–CO<sub>2</sub> fluids, Mt Isa, Australia. *Geochim. Cosmochim. Acta* **2011**, *75*, 1428–1450. [[CrossRef](#)]
65. Kendrick, M.A.; Honda, M.; Walshe, J.; Petersen, K. Fluid sources and the role of abiogenic-CH<sub>4</sub> in Archean gold mineralization: Constraints from noble gases and halogens. *Precambrian Res.* **2011**, *189*, 313–327. [[CrossRef](#)]
66. Blamey, N.J.F. Composition and evolution of crustal, geothermal and hydrothermal fluids interpreted using quantitative fluid inclusion gas analysis. *J. Geochem. Explor.* **2012**, *116–117*, 17–27. [[CrossRef](#)]
67. Cawood, P.A.; Zhao, G.; Yao, J.; Wang, W.; Xu, Y.; Wang, Y. Reconstructing South China in Phanerozoic and Precambrian supercontinents. *Earth-Sci. Rev.* **2018**, *186*, 173–194. [[CrossRef](#)]
68. Shu, L. Predevonian tectonic evolution of South China: From Cathaysian Block to Caledonian period folded orogenic belt. *Geol. J. China Univ.* **2006**, *12*, 418–431. (In Chinese)
69. Li, S.; Zhao, S.; Liu, X.; Cao, H.; Yu, S.; Li, X.; Somerville, I.; Yu, S.; Suo, Y. Closure of the Proto-Tethys Ocean and Early Paleozoic amalgamation of microcontinental blocks in East Asia. *Earth-Sci. Rev.* **2018**, *186*, 37–75. [[CrossRef](#)]
70. Zhao, G.; Wang, Y.; Huang, B.; Dong, Y.; Li, S.; Zhang, G.; Yu, S. Geological reconstructions of the East Asian blocks: From the breakup of Rodinia to the assembly of Pangea. *Earth-Sci. Rev.* **2018**, *186*, 262–286. [[CrossRef](#)]

71. Li, Z.; Li, X.; Wartho, J.A.; Clark, C.; Li, W.; Zhang, C.; Bao, C. Magmatic and metamorphic events during the early Paleozoic Wuyi-Yunkai orogeny, southeastern South China: New age constraints and pressure-temperature conditions. *Geol. Soc. Am. Bull.* **2010**, *122*, 772–793. [[CrossRef](#)]
72. Guo, R.; Peng, E. Regional geological background, ore-forming characters and metallogeny of Songxi silver deposit, east Guagdong. *Geotect. Metall.* **2009**, *33*, 567–572. (In Chinese)
73. Chen, Y.; Liang, B.; Liao, L. Major characteristics of carboniferous sedimentary facies of Yushui-Yinshi district in Meixian County, Guangdong Province. *Guangdong Geol.* **1992**, *7*, 27–39. (In Chinese)
74. Leach, D.L.; Sangster, D.F.; Kelley, K.D.; Large, R.R.; Garven, G.; Allen, C.R.; Gutzmer, J.; Walters, S. Sediment-hosted lead-zinc deposits: A global perspective. *Econ. Geol.* **2005**, *100*, 561–607.
75. Leach, D.L.; Bradley, D.C.; Huston, D.; Pisarevsky, S.A.; Taylor, R.D.; Gardoll, S.J. Sediment-hosted lead-zinc deposits in Earth History. *Econ. Geol.* **2010**, *105*, 593–625. [[CrossRef](#)]
76. Hu, R.; Bi, X.; Jiang, G.; Chen, H.; Peng, J.; Qi, Y.; Wu, L.; Wei, W. Mantle-derived noble gases in ore-forming fluids of the granite-related Yaogangxian tungsten deposit, Southeastern China. *Miner. Depos.* **2012**, *47*, 623–632. [[CrossRef](#)]
77. Li, J.; Li, J.; Liu, H.; Zhang, J.; Jin, G.; Zhang, J.; Han, J. Helium isotope composition of inclusions in mineral grains using Helix SFT noble gas mass spectrometer. *Acta Geol. Sin.* **2015**, *89*, 1826–1831. (In Chinese)
78. Xie, G.; Mao, J.; Li, W.; Zhu, Q.; Liu, H.; Jia, G.; Li, Y.; Li, J.; Zhang, J. Different proportion of mantle-derived noble gases in the Cu-Fe and Fe skarn deposits: He-Ar isotopic constraint in the Edong district, Eastern China. *Ore Geol. Rev.* **2016**, *72*, 343–354. [[CrossRef](#)]
79. Allègre, C.J.; Staudacher, T.; Sarda, P. Rare gas systematics: Formation of the atmosphere, evolution and structure of the earth's mantle. *Earth Planet. Sci. Lett.* **1987**, *81*, 127–150. [[CrossRef](#)]
80. Andrews, J.N. The isotopic composition of radiogenic helium and its use to study groundwater movement in confined aquifers. *Chem. Geol.* **1985**, *49*, 339–351. [[CrossRef](#)]
81. Patterson, D.B.; Honda, M.; McDougall, I. Noble gases in mafic phenocrysts and xenoliths from New Zealand. *Geochim. Cosmochim. Acta* **1994**, *58*, 4411–4427. [[CrossRef](#)]
82. Dunai, T.J.; Baur, H. Helium, neon and argon systematics of the European subcontinental mantle: Implications for its geochemical evolution. *Geochim. Cosmochim. Acta* **1995**, *59*, 2767–2783. [[CrossRef](#)]
83. Reid, M.R.; Graham, D.W. Resolving lithospheric and sub-lithospheric contributions to helium isotope variations in basalts from the southwestern US. *Earth Planet. Sci. Lett.* **1996**, *144*, 213–222. [[CrossRef](#)]
84. Ballentine, C.J.; Burgess, R.; Marty, B. Tracing fluid origin, transport and interaction in the crust. *Rev. Mineral. Geochem.* **2002**, *47*, 539–614. [[CrossRef](#)]
85. Torgersen, T.; Kennedy, B.M.; Hiyagon, H.; Chiou, K.Y.; Reynolds, J.H.; Clarke, W.B. Argon accumulation and the crustal degassing flux of  $^{40}\text{Ar}$  in the Great Artesian Basin, Australia. *Earth Planet. Sci. Lett.* **1989**, *92*, 43–56. [[CrossRef](#)]
86. Huizenga, J.-M. Thermodynamic modelling of C–O–H fluids. *Lithos* **2001**, *55*, 101–114. [[CrossRef](#)]
87. Potter, J.; Konnerup-Madsen, J. A review of the occurrence and origin of abiogenic hydrocarbons in igneous rocks. *Geol. Soc. London Spec. Publ.* **2003**, *214*, 151–173. [[CrossRef](#)]
88. Konnerup-Madsen, J.; Rose-Hansen, J. Volatiles associated with alkaline igneous rift activity: Fluid inclusions in the Ilímaussaq Intrusion and the Gardar granitic complexes (south Greenland). *Chem. Geol.* **1982**, *37*, 79–93. [[CrossRef](#)]
89. Hou, Z.; Zhang, Q. CO<sub>2</sub>-Hydrocarbon fluids of the Jade hydrothermal field in the Okinawa Trough: Fluid inclusion evidence. *Sci. China Ser. D Earth Sci.* **1998**, *41*, 408–415. [[CrossRef](#)]
90. Wilkinson, J.J. Fluid inclusions in hydrothermal ore deposits. *Lithos* **2001**, *55*, 229–272. [[CrossRef](#)]
91. Kesler, S.E. Ore-forming fluids. *Elements* **2005**, *1*, 13–18. [[CrossRef](#)]
92. Norman, D.I.; Moore, J.N. Methane and excess N<sub>2</sub> and Ar in geothermal fluid inclusions. In Proceedings of the Twenty-Third Workshop on Geothermal Reservoir Engineering, Stanford University, Stanford, CA, USA, 25–27 January 1999.
93. Barré, G.; Truche, L.; Bazarkina, E.F.; Michels, R.; Dubessy, J. First evidence of the trisulfur radical ion S<sub>3</sub><sup>-</sup> and other sulfur polymers in natural fluid inclusions. *Chem. Geol.* **2017**, *462*, 1–14. [[CrossRef](#)]
94. Goldstein, T.P.; Aizenshtat, Z. Thermochemical sulfate reduction: A review. *J. Therm. Anal.* **1994**, *42*, 241–290. [[CrossRef](#)]
95. Machel, H.G.; Krouse, H.R.; Sassen, R. Products and distinguishing criteria of bacterial and thermochemical sulfate reduction. *Appl. Geochem.* **1995**, *10*, 373–389. [[CrossRef](#)]

96. Machel, H.G. Bacterial and thermochemical sulfate reduction in diagenetic settings—Old and new insights. *Sediment. Geol.* **2001**, *140*, 143–175. [[CrossRef](#)]
97. Basuki, N.; Taylor, B.E.; Spooner, E.T.C. Sulfur isotope evidence for thermochemical reduction of dissolved sulfate in Mississippi Valley-type zinc-lead mineralization, Bongara Area, Northern Peru. *Econ. Geol.* **2008**, *103*, 783–799. [[CrossRef](#)]
98. Thom, J.; Anderson, G.M. The role of thermochemical sulfate reduction in the origin of Mississippi Valley-type deposits. I. Experimental results. *Geofluids* **2008**, *8*, 16–26. [[CrossRef](#)]
99. Gadd, M.G.; Layton-Matthews, D.; Peter, J.M.; Paradis, S.; Jonasson, I.R. The world-class Howard’s Pass SEDEX Zn-Pb district, Selwyn Basin, Yukon. Part II: the roles of thermochemical and bacterial sulfate reduction in metal fixation. *Miner. Depos.* **2017**, *52*, 405–419. [[CrossRef](#)]
100. Kerrick, D.M.; Connolly, J.A.D. Metamorphic devolatilization of subducted marine sediments and the transport of volatiles into the Earth’s mantle. *Nature* **2010**, *411*, 293–296. [[CrossRef](#)]
101. Hu, W.; Kang, X.; Cao, J.; Wang, X.; Fu, B.; Wu, H. Thermochemical oxidation of methane induced by high-valence metal oxides in a sedimentary basin. *Nat. Commun.* **2018**, *9*, 5131. [[CrossRef](#)]
102. Liu, Q.Y.; Worden, R.H.; Jin, Z.J.; Liu, W.H.; Li, J.; Gao, B.; Zhang, D.W.; Hu, A.P.; Yang, C. TSR versus non-TSR processes and their impact on gas geochemistry and carbon stable isotopes in Carboniferous, Permian and Lower Triassic marine carbonate gas reservoirs in the Eastern Sichuan Basin, China. *Geochim. Cosmochim. Acta* **2013**, *100*, 96–115. [[CrossRef](#)]
103. Tarantola, A.; Mullis, J.; Vennemann, T.; Dubessy, J.; de Capitani, C. Oxidation of methane at the CH<sub>4</sub>/H<sub>2</sub>O–(CO<sub>2</sub>) transition zone in the external part of the Central Alps, Switzerland: Evidence from stable isotope investigations. *Chem. Geol.* **2007**, *237*, 329–357. [[CrossRef](#)]
104. Tarantola, A.; Mullis, J.; Guillaume, D.; Dubessy, J.; de Capitani, C.; Abdelmoula, M. Oxidation of CH<sub>4</sub> to CO<sub>2</sub> and H<sub>2</sub>O by chloritization of detrital biotite at 270 ± 5 °C in the external part of the Central Alps, Switzerland. *Lithos* **2009**, *112*, 497–510. [[CrossRef](#)]
105. Lu, H.; Liu, C. Formation of strata-bound ore deposits in China: Studies on fluid inclusions. *Chin. J. Geochem.* **1990**, *9*, 347–360. (In Chinese)
106. Roedder, E. Fluid inclusions. *Rev. Mineral.* **1984**, *12*, 1–644.
107. Cai, J.; Liu, J. Characteristics of structures and prospecting targets in the metallogenic province at the south sector of Yongmei depression, Guangdong. *Geotect. Metall.* **1996**, *20*, 333–339. (In Chinese)
108. Essarraj, S.; Boiron, M.-C.; Cathelineau, M.; Tarantola, A.; Leisen, M.; Boulvais, P.; Maacha, L. Basinal brines at the origin of the Imiter Ag-Hg deposit (Anti-Atlas, Morocco): Evidence from LA-ICP-MS data on fluid inclusions, halogen signatures, and stable isotopes (H, C, O). *Econ. Geol.* **2016**, *111*, 1753–1781. [[CrossRef](#)]



© 2019 by the authors. Licensee MDPI, Basel, Switzerland. This article is an open access article distributed under the terms and conditions of the Creative Commons Attribution (CC BY) license (<http://creativecommons.org/licenses/by/4.0/>).